Energy Conversion and Management 271 (2022) 116325

Contents lists available at ScienceDirect

Energy Conversion and Management

journal homepage: www.elsevier.com/locate/enconman

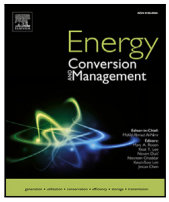

# Comparison of cryogenic and membrane oxygen production implemented in the Graz cycle

Fabio Alberto Gutiérrez [a,*], Luis Miguel García-Cuevas [a], Wolfgang Sanz [b]

[a] CMT – Motores Térmicos, Universitat Politècnica de València. Camino de Vera s/n, Valencia, 46022, Valencia, Spain
[b] Institute of Thermal Turbomachinery and Machine Dynamics. TU Graz. Inffeldgasse 25/A, Graz, A-8010, Graz, Austria

ARTICLE INFO

*Keywords:*
Oxygen
Membrane
Oxy-fuel
$O_2$ production
Graz cycle

ABSTRACT

One of the most promising technologies to decrease greenhouse gas emissions is carbon capture and storage (CCS). Oxy-fuel combustion, in which high-purity oxygen mixed with flue gases is used to burn fuels, reduces the complexity of CCS systems. Several methods have been studied for oxygen production to feed the process, where cryogenic air separation is the most mature technology. However, it is a highly energy-intensive method, which motivates the research of other alternatives such as ceramic membranes.

In order to compare the performance of both oxygen separation methods, the coupling of an oxygen production cycle based on ceramic membranes with a high-efficient power cycle, the Graz cycle, is studied. This cycle initially operates using cryogenic air separation.

The calculations of both cycles are carried out using the simulation software IPSEpro. For the membrane cycle, two cases are identified, whose main difference is the method to reduce the oxygen partial pressure on the permeate side of the membrane: vacuum generation (Case 1) and membrane sweeping (Case 2). Both cases are optimized, considering the thermodynamic conditions of the membrane operation and its effects on the energy consumption of oxygen production. Membrane cases achieve 54.08% and 55.76% of net efficiency for Case 1 and 2, respectively, being 0.61% and 2.30% points higher than the base case. Furthermore, the differences in turbomachine performances and streams variations are discussed, considering the effects of energy integration of membrane cases.

## 1. Introduction

Currently, one of the challenges in the industry is the reduction of pollutant and greenhouse gas emissions. The International Energy Agency (IEA) [1] reports that pre-COVID levels of emissions will be reached again around 2023–2025 due to the recovery of economic activities.

In this sense, the power production sector is one of the leading sectors of pollutant gases production. In the European Union (EU), approximately 21 % of the total energy consumption is by means of electricity, whereas 40 % is generated burning fossil fuels [2]. Thereupon, governmental frameworks were introduced whose purpose is the reduction of pollutant and greenhouse gas emissions. The EU has presented the 2050 long-term strategy, aiming to be climate neutral by 2050, aligning with the actions proposed in the Paris agreement [3].

One of the strategies to reduce the emission of greenhouse gases such as $CO_2$ is Carbon Dioxide Capturing and Storage (CCS), which is a promising procedure in which $CO_2$ is separated, transported and stored in long-term storage isolated from the atmosphere [4]. The authors expect CCS technologies to be a key in some industrial sectors as cement production, where 60 % of the $CO_2$ production is unavoidable due to the nature of calcination, an important part of the process [5]; also, in the power production sector, where most of the thermal energy sources are fossil fuels like coal and natural gas [6].

From this perspective, oxy-fuel combustion is seen as one of the most promising technologies to enable easy sequestration of $CO_2$ in industry. In oxy-fuel combustion, the combustion is performed using a mixture of oxygen and a thermal buffer (normally recycled flue gas composed of a $CO_2/H_2O$ mixture), used to control the combustor temperatures instead of regular air. This removes nitrogen from the process, leading to a flue gas of higher $CO_2$ concentration, where $CO_2$ can be easily captured after a previous dehydration [7]. In addition to that, it has been reported that oxy-fuel combustion almost totally avoids NOx production, which can be up to 40 times smaller than with conventional combustion when using the same oxygen content, due to the removal of nitrogen from the comburent [8].

* Corresponding author.
*E-mail address:* fagucas@posgrado.upv.es (F.A. Gutiérrez).
*URL:* https://www.cmt.upv.es/ (F.A. Gutiérrez).

https://doi.org/10.1016/j.enconman.2022.116325
Received 20 July 2022; Received in revised form 23 September 2022; Accepted 3 October 2022
Available online 20 October 2022

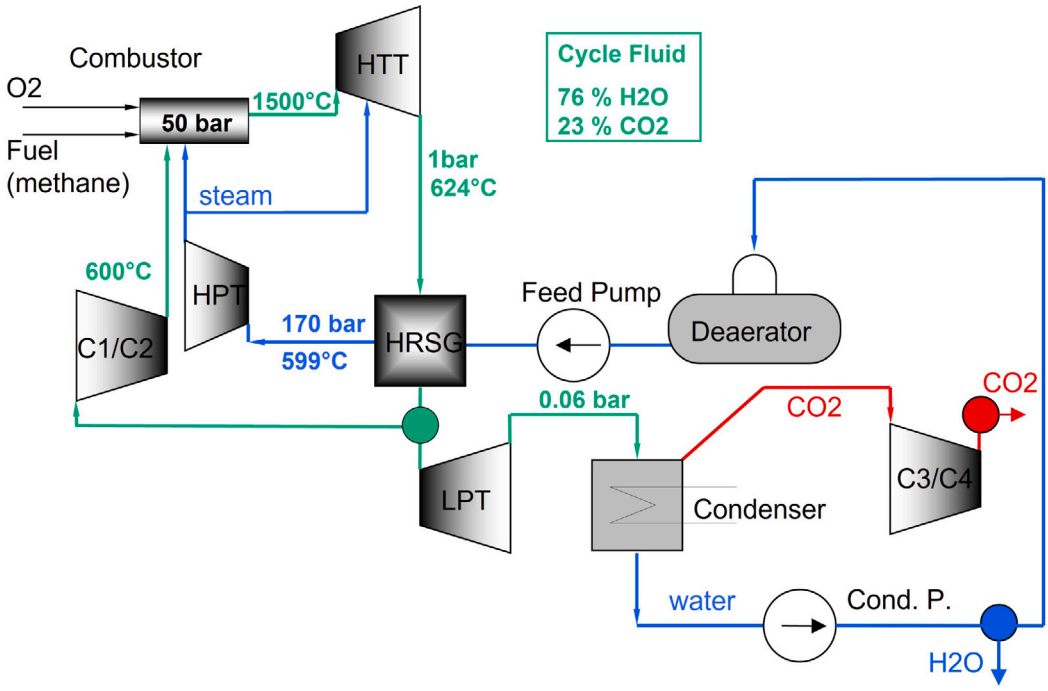


**Fig. 1.** Flow scheme of the Graz Cycle.
*Source:* Taken from [11].

Oxy-fuel combustion has been studied for different types of fuels, exhibiting acceptable cycle efficiencies and high rates of carbon capture. Shi et al. [9] studied the use of different solid fuels as coal, lignite and sawdust in oxy-combustion power plants: for all cases, more than 97 % of the $CO_2$ could be captured during this operation. An oxy-combustion liquefied natural gas (LNG) power plant was studied by Liang et al. [10], where two auxiliary power generation sub-systems were also implemented. They compared the combustion in $O_2/CO_2$ and $O_2/H_2O$ atmospheres, which were chosen as thermal buffer gases. Efficiencies of 58.78 % were reached in the study, where 94.8 % of the $CO_2$ was captured with a purity of 97.2 %.

A study similar to the case above was performed with natural gas as fuel by Cai et al. [12], using an auxiliary subsystem of power production, and performing the combustion using recycled flue gas, pure $CO_2$ or steam mixed as alternative thermal buffers. A purity of 98 % was obtained for the captured $CO_2$, achieving a maximum cycle efficiency of 67.6 % for the $O_2$/recycled flue gases case due to the high temperature of recirculation, exhibiting as the best option in this study.

In these mentioned cases, high-purity oxygen production was performed using cryogenic methods, the most common method in industry. In this method, the air is separated in a multi-column cryogenic distillation process by taking advantage of the different boiling temperatures of its main components, nitrogen and oxygen. The state-of-the-art method can produce oxygen with a purity of 99.5 %, recovering 97.85 % of the oxygen in the air. However, this is a highly energy-intensive method, causing a penalty of 3 % to 4 % of input energy and an efficiency reduction up to 8.5 % in processes where oxy-fuel combustion is applied [13].

For this reason, another oxygen production method studied to improve oxy-fuel cycle efficiencies is the use of ceramic membranes. Due to a pressure gradient between the feed and permeate sides, these membranes have an oxygen diffusion process through their crystal lattice, favored by high temperatures (preferably > 700 °C), which increase the vacancy sites in the lattice, improving the oxygen flux [14]. There are two different modes of operation for these membranes, called 3-end and 4-end, which differ in the method to create the required differential oxygen partial pressure. The driving force for the 3-end is created by generating a vacuum in the permeate side, while for the 4-end a sweeping gas is used in the permeate side to reduce the oxygen concentration, creating the partial pressure gradient [15].

Skorek-Osikowska et al. [16] presented two cases for a 460 MW oxy-fuel combustion power plant where the integration of a hybrid membrane-cryogenic installation was compared with a cryogenic air separation unit, both used for oxygen production. After a thermodynamic evaluation, it was found that the addition of a membrane to the system improved the first law efficiency by 1.1 %, reducing the auxiliary power consumption by 13 %. Portillo et al. [15] compared the performance of cryogenic and membrane methods to produce oxygen for a coal-power plant. They found a 5 % improvement in the energy efficiency and a lower specific $CO_2$ capture when membranes were used compared with the cryogenic case. Additionally, an advanced zero-emission power plant using a ceramic membrane to produce oxygen was studied by Gunasekaran et al. [7], where the influence of the membrane operation temperature was examined evaluating quantities such as power plant production and efficiency. Maximum efficiency of 53.2 % was achieved for 850 °C membrane temperature capturing 100 % of the $CO_2$ produced during the operation of the plant, where it was found that reducing the temperature could be favorable in terms of efficiency, but drastically affecting the power output as the oxygen production for fuel combustion is affected.

This being said, it is seen that the implementation of membranes could improve an existent oxy-fuel power plant efficiency when the oxygen production is performed using cryogenic methods. In these cases, a proper energetic integration could improve the power plant efficiency, making it more competitive. In fact, membrane implementation can be performed in systems where it is required to reduce pollutant emissions and high-temperature streams are presented to feed the membrane, as it is seen in Serrano et al. [17]

Considering this, a study on the Graz Cycle is performed, which is an oxyfuel power cycle of highest efficiency developed at Graz University of Technology [18–24], whose primary oxygen source is a cryogenic air separation installation. An oxygen production cycle based on a mixed ionic–electronic conducting (MIEC) ceramic-based membrane is integrated into the cycle to produce the required oxygen instead of

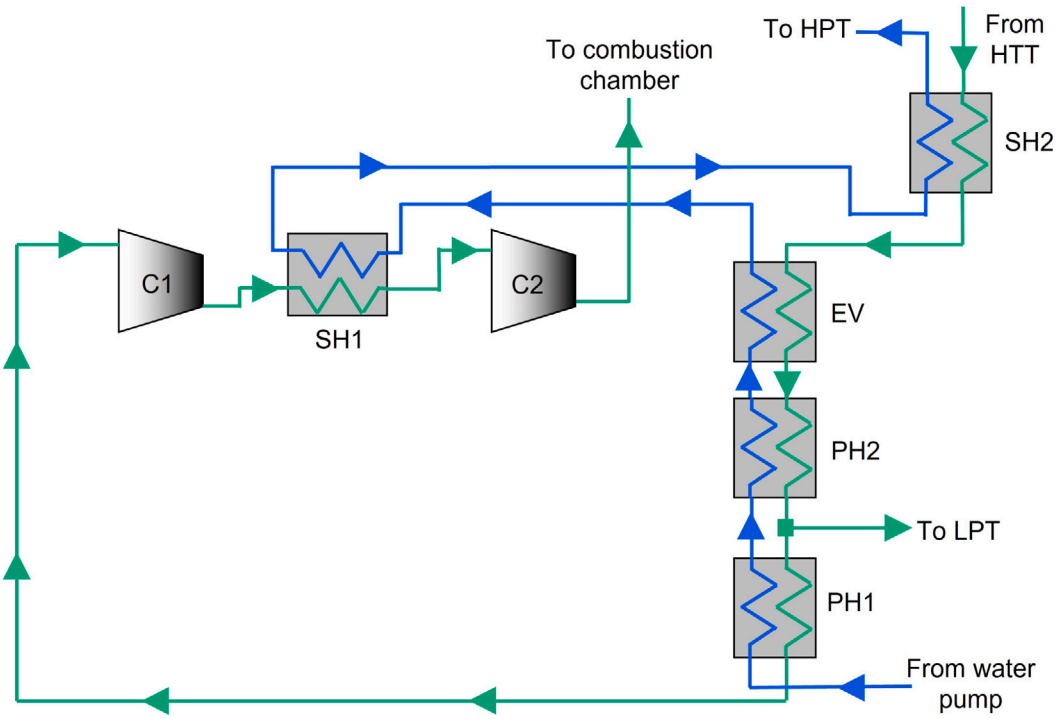


**Fig. 2.** Flow scheme of the HRSG of the Graz Cycle.
*Source:* Adapted from [11].

the original method, considering the alternatives of 3-end and 4- end membranes. Therefore, a comparative study of three cases is presented: a base case as it was determined in its last optimization [11], where a cryogenic process is implemented for oxygen production; a case where a 3-end membrane is used in the oxygen production cycle (Case 1), and a case where a 4-end membrane is implemented (Case 2).

The main objectives of this paper are:

- Optimize the main operation parameters of an oxygen production cycle using membranes coupled to the Graz Cycle for both proposed cases.
- Compare the performance of the three mentioned cases, considering the power plant production, the efficiency of the whole system and the energy cost of oxygen production.

## 2. Process description

### 2.1. Base case

The Graz Cycle consists basically of two coupled cycles: a high-temperature Brayton cycle (Compressors C1/C2, combustion chamber (CC) and High-Temperature Turbine (HTT)), and a low-temperature Rankine cycle (Low-Pressure Turbine (LPT), condenser, Heat Recovery Steam Generator (HRSG) and a High-Pressure Turbine (HPT). Fig. 1 exhibits a flow scheme of the Graz cycle. For more details, refer to the article by Wimmer and Sanz [11] where the last optimization of the cycle was performed.

A combustion chamber is run at 50 bar, operating with natural gas and an atmosphere of high purity oxygen, which is produced via cryogenic distillation, steam, and recycled working fluid, where a stream with a composition of 76 % water, 23 %$CO_2$ and residual components as nitrogen and argon is produced. This composition is orientative, which could change around this values as modifications in the cycle are performed, as coupling other oxygen production method. This working fluid leaves the combustor at 1500 °C, being expanded in the HTT, which is cooled by steam from the HPT outlet flow, increasing the steam content of HTT stream. Then, the gases are cooled in the HRSG to vaporize and superheat the water for the HPT. The HRSG scheme used in the Graz cycle is shown in Fig. 2

**Table 1**
Main thermodynamic conditions of Graz Cycle.

| | |
|---|---|
| Power plant output | 400 MW |
| Fuel consumption | 16.09 kg/s |
| HTT inlet temperature | 1500 °C |
| HPT inlet pressure | 17 MPa |
| LPT inlet pressure | 0.1 MPa |
| Condensation pressure | 6 kPa |
| Combustion chamber pressure | 5 MPa |
| Thermal electric efficiency | 65.82 % |
| Efficiency considering $O_2$ supply | 56.00 % |
| Efficiency considering $O_2$ supply and $CO_2$ compression | 53.47 % |

After this, this gas is branched, where about half of the mass flow is compressed in C1/C2, feeding the CC to regulate its temperature. On the other hand, the other half of the gases is driven through the LPT and then is condensed in several stages. $CO_2$ and water are separated, and $CO_2$ is compressed in C3/C4, captured afterwards. The condensed water is pumped and superheated in the HRSG, and finally goes into the HPT, whose outlet flow is divided for HTT and CC cooling.

Table 1 highlights the main thermodynamic conditions of the cycle:

### 2.2. Case 1: 3-end membrane

Fig. 3(a) shows an oxygen production cycle based on a 3-end membrane coupled to the Graz cycle. The oxygen production cycle consists of a group of turbochargers and heat exchangers that allows the air to reach the optimal pressure and temperature conditions at the feed side. First, atmospheric air (1 bar, 25 °C) is driven through the cycle by three intercooled mechanical compressors (LPC, MPC, HPC) and an electric compressor (EC) used to boost the air pressure. After that, two heat exchangers (HE-1 and HE-2) are implemented to recover energy from the outlet streams of the membrane, increasing the air temperature.

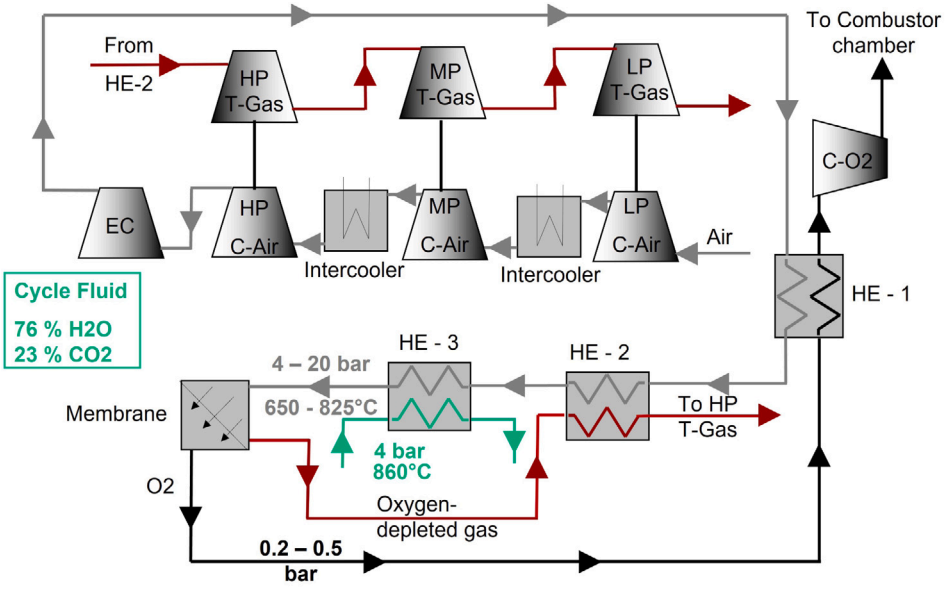


(a) Flow scheme of a oxygen production cycle with a 3-end membrane.

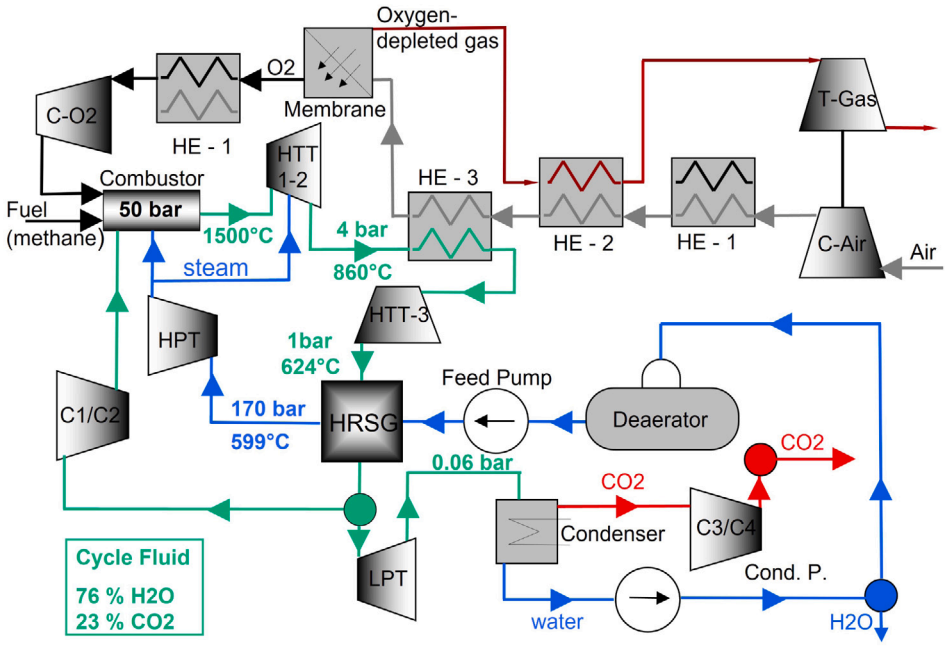


(b) Flow scheme of Graz cycle with a 3-end membrane oxygen production cycle.

**Fig. 3.** Flow scheme of Graz cycle — Case 1.

Then, the air is finally heated in a heat exchanger (HE-3) coupled with the Graz cycle; the stream after the last cooled stage of HTT at 860 °C is used to increase the air temperature before it goes into the membrane.

In the membrane, working at 4 bar to 20 bar and 650 °C to 825 °C, the differential partial pressure and high temperature induce the oxygen separation from the air, splitting it into two streams: First, the high-purity oxygen, whose line is firstly at vacuum pressure to promote its production. The oxygen leaves the membrane at a high temperature, whereby it is used to increase the air temperature (HE-1). Then, it is compressed in C-O2, right before being compressed to CC conditions. Second, the oxygen-depleted stream (mainly nitrogen) heats the air mass flow (HE-2) and then it is used in three expansion stages (LPT, MPT, HPT) to drive the mechanical compressors. The whole system, oxygen production and Graz cycle coupled, is shown in Fig. 3(b). For clarity, heat exchanger HE-1 is depicted twice. It is worth to mention that this case uses the same configuration for the HRSG as it is shown in Fig. 2

### 2.3. Case 2: 4-end membrane

Fig. 4(a) shows an isolated oxygen production cycle operating with a 4-end membrane. The 4-end membrane case shares many similarities with the 3-end, with the difference that a swept membrane is implemented, where the recycled gas used in the CC is previously used to sweep the permeate side of the membrane.

This gas is taken from the C1 outlet, composed primarily of $CO_2$ and steam, at a pressure of 15 bar and a temperature around 480 °C. This diminishes the oxygen partial pressure due to the very low oxygen

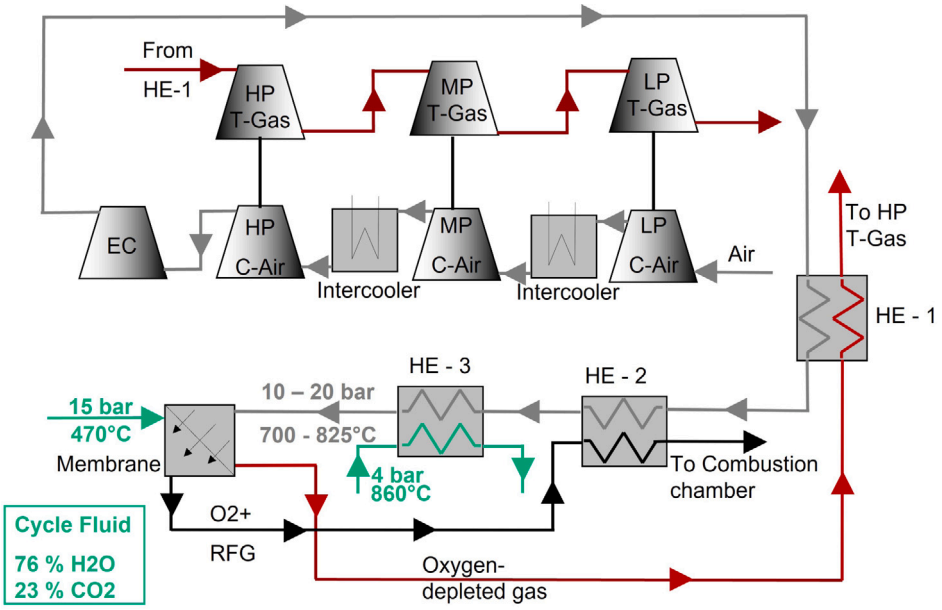


(a) Flow scheme of a oxygen production cycle with a 4-end membrane.

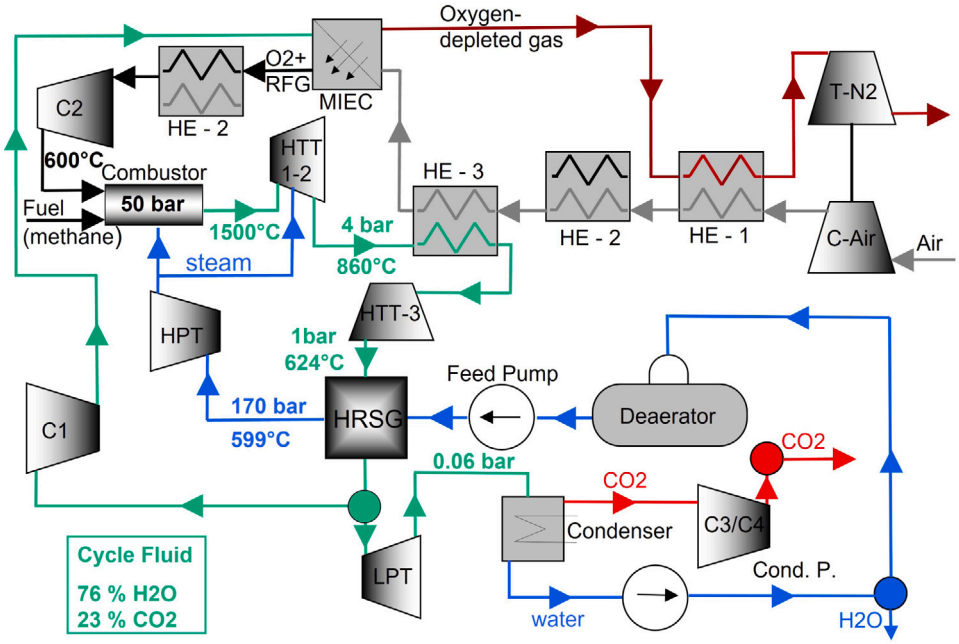


(b) Flow scheme of Graz cycle with a 4-end membrane oxygen production cycle.

**Fig. 4.** Flow scheme of Graz cycle — Case 2.

content, not being necessary to create a vacuum in the oxygen line. Therefore, the three compression stages in the oxygen line are eliminated, using C2 to reach the 50 bar at the CC. Before C2, the O2/RFG mixture goes through the HRSG of the Graz Cycle, superheating the steam flow at the SH1 heat exchanger, as it is shown in Fig. 5. The configuration of this case can be seen in Fig. 4(b), where heat exchanger HE-2 is depicted twice for clarity.

## 3. Methodology

The required calculations are performed by using IPSEpro v8 from Simtech Simulation Technology [25], which is a software used to model and analyze different types of processes in engineering. Additionally, the model library of the oxyfuel processes was extended by the membrane models

### 3.1. Thermodynamic models and assumptions

To perform this study, the following models and assumptions were considered:

- Regarding the Graz Cycle, its calculation is performed as in the article by Wimmer and Sanz [11], where all the assumptions, modeling of the components, and considerations were taken from.

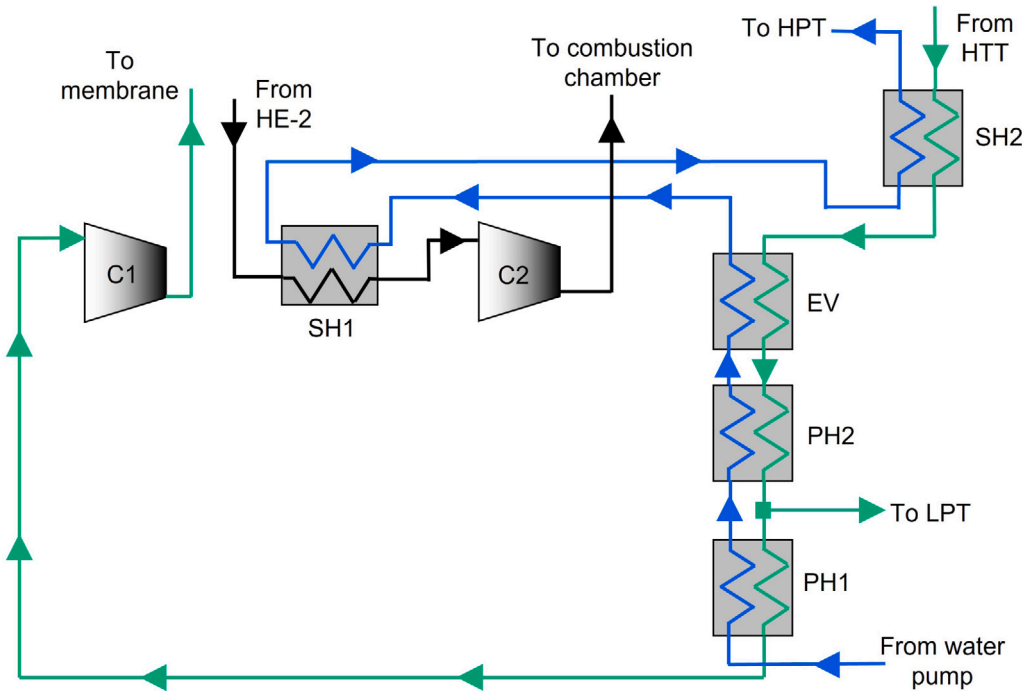


**Fig. 5.** Flow scheme of the HRSG of the Graz cycle for Case 2.
*Source:* Adapted from [11].

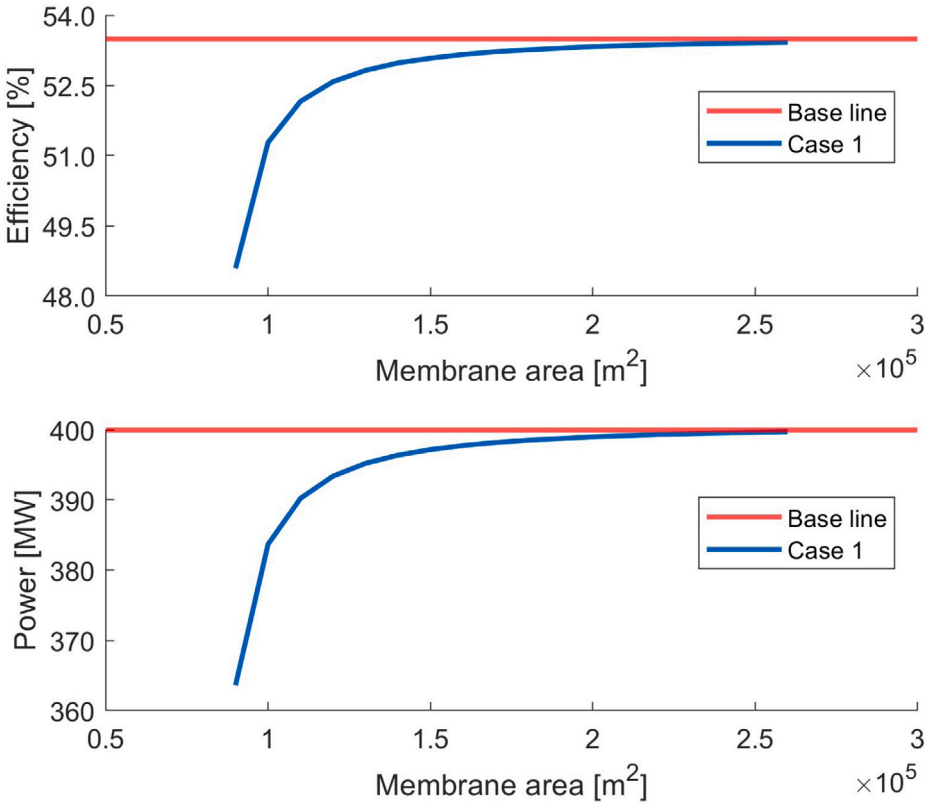


**Fig. 6.** Thermal efficiency and power variation with membrane area — Medium conditions — Case 1.

- The effort of $CO_2$ compression performed at C3/C4 to CCS conditions (110 bar and 30 °C) is considered to be 114 kJ kg$^{-1}$ as it is stated by Wimmer and Sanz [11].
- For the base case, $O_2$ production is delivered from the cryogenic distillation cycle at 16 bar and 15 °C, requiring a specific work of 1049 kJ kg$^{-1}$. For the membrane cases, oxygen is delivered around 16 bar. After this, for all cases, the oxygen is compressed to CC conditions.
- Oxygen permeation in the membrane is calculated following the one dimensional equations proposed by Catalán-Martínez et al.

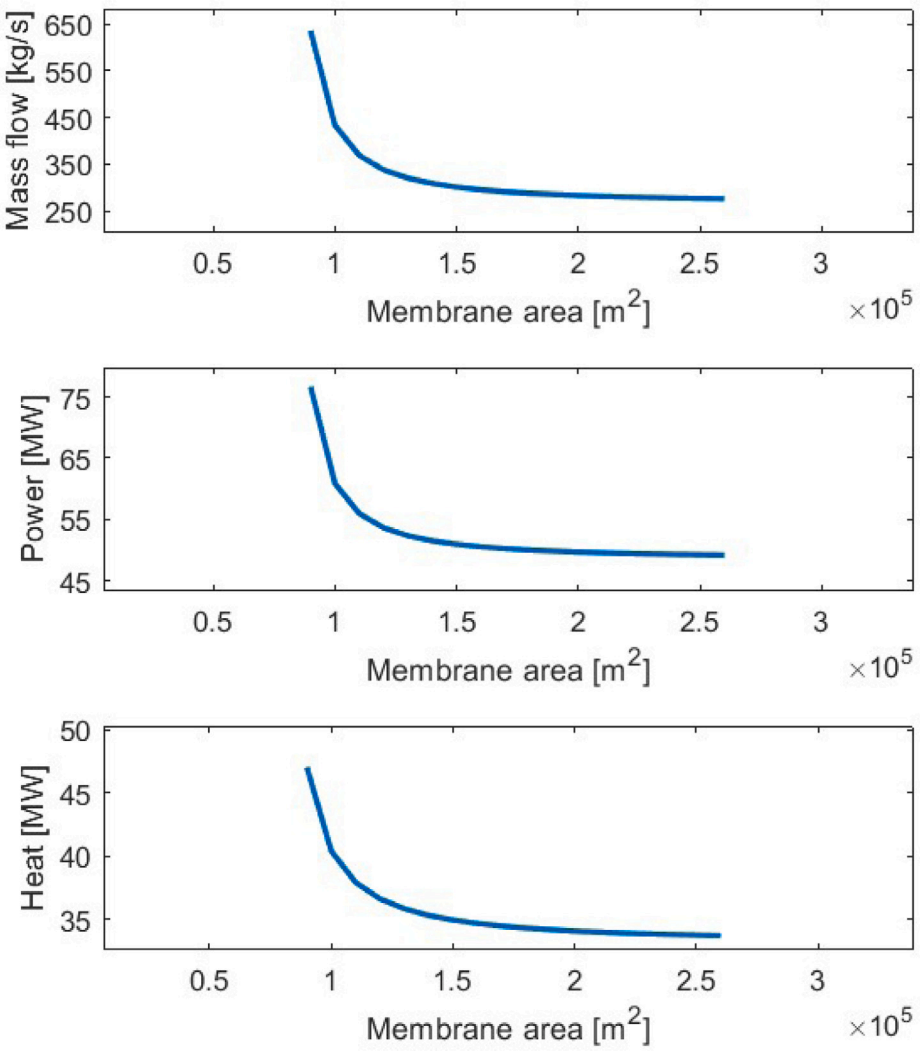


**Fig. 7.** Variation of air mass flow, electric power consumption and heat from GC variation with membrane area — Medium conditions — Case 1.

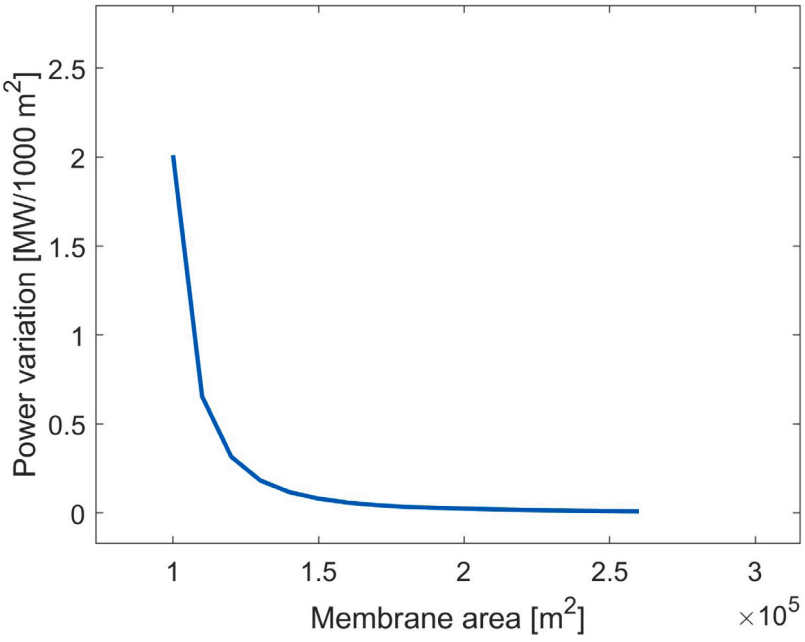


**Fig. 8.** Change of power increase variation with membrane area — Medium conditions – Case 1.

**Table 2**
Turbomachine efficiencies.

| | |
|---|---|
| Turbocharger compressors | 84 % |
| Turbocharger turbines | 88 % |
| High-pressure electric compressor | 84 % |
| Oxygen line compressors (Case 1) | 82.8 % |

[26], considering a $Ba_{0.5}Sr_{0.5}Co_{0.8}Fe_{0.2}O_{3-\delta}$ (BSCF) membrane and an isothermal model according to Wagner's equation (see Eq. (1)).

$$\dot{m}_{O_2} = \frac{C \cdot e^{\left(\frac{-K}{T}\right)} \cdot \ln\left(\frac{P_{O_2,f}}{P_{O_2,p}}\right) \cdot T \cdot MW_{O_2} \cdot A}{L} \quad (1)$$

where $C$ and $K$ are membrane material constants whose values are $1.004 \times 10^{-8}$ mol cm $s^{-1}$ and 6201 K, respectively. $T$ is the operation temperature of the membrane, $MW_{O_2}$ is the molecular weight of the oxygen, $A$ is the membrane area and $L$ is the membrane thickness. This thickness is set to 200 μm, reproducing the results of a thin-layer membrane supported by a porous BSCF substrate with a total thickness of 900 μm.

$P_{O_2,f}$ is the mean oxygen partial pressure at the feed side and $P_{O_2,p}$, the mean partial pressure at the permeate side. The mean partial pressures are determined by the geometric mean of oxygen partial pressure of inlet and outlet streams for both feed and permeate sides of the membrane, calculated as shown in Eqs. (2) and (4)

Feed pressure:

$$P_{O_2,f} = P_f \cdot X_{O_2,f} \quad (2)$$

$$X_{O_2,f} = \sqrt{X_{O_2,in,f} \cdot X_{O_2,out,f}} \quad (3)$$

Permeate pressure:

$$P_{O_2,p} = P_p \cdot X_{O_2,p} \quad (4)$$

$$X_{O_2,p} = 1 - \sqrt{(1 - X_{O_2,in,f}) \cdot (1 - X_{O_2,out,f})} \quad (5)$$

The membrane is supported by a BSCF porous substrate, as described by Baumann et al. [27].

- A temperature difference of 25 °C is set for HE-1 and HE-2 in both membrane-based cases. For HE-3, an outlet air temperature is imposed.
- For the oxygen production cycle, isentropic and mechanical efficiencies for turbomachines remain constant. Table 2 contains the values for each of them.
- Pressure drop in the heat exchangers for the oxygen production cycle are set to be 1 % of the inlet pressure for each flow.
- Equal pressure ratios for the expansion stages in the oxygen production cycle are considered.

### 3.2. Parameter evaluation of the oxygen production cycle

Different operating conditions of the air separation membrane for the two cases studied are examined, researching how this affects the performance of the whole system. For Case 1, the performance of the coupling of Graz cycle and oxygen production cycle is studied for changes in the feed pressure and temperature and the vacuum pressure. The following ranges for the variables mentioned above are considered:

- Feed air pressure: [4–20] bar
- Vacuum pressure: [0.2–0.5] bar
- Feed air temperature [650–825] °C

**Table 3**
Mean used conditions to determine membrane area.

| | Case 1 (3-end membrane) | Case 2 (4-end membrane) |
|---|---|---|
| Feed air pressure [bar] | 12 | 15 |
| Feed air temperature [°C] | 750 | 750 |
| Vacuum pressure [bar] | 0.35 | *** |

For Case 2, as the oxygen partial pressure is not directly controlled at the permeate side, the study is performed by considering different feed pressure and temperature conditions at the membrane.

- Feed air pressure: [10–20] bar
- Feed air temperature: [700–825] °C

These operation ranges are considered as maximum air feed pressures of 20 bar are found in the literature. According to Zhu and Yang [28], the sealing of this type of membrane at higher pressures than 20 bar is still a technological challenge. On the other hand, the membranes have practical applications when operating between 700–1000 °C, although there are studies where lower temperatures (less than 500 °C) are being developed [28].

Additionally, to determine the membrane area used in the analysis of both cases, the studied ranges are taken as a reference, where mean conditions are chosen to select an appropriate size for each studied case, which remains constant as the membrane area is varied. The used conditions are presented in Table 3.The selected areas for each case are determined to achieve the maximum power and thermal efficiency under the imposed feed and permeate membrane conditions, considering the inherent difficulties of operating with excessive membrane sizes and, also, to obtain a considerable amount of operative points for the studied ranges in each case.

Furthermore, both cases consider that the outlet temperature of each cooler is 25 °C. Nonetheless, the variation of this temperature modifies the heat required from HE-3 and the electric power consumption of the compressors. For this reason, the system behavior is studied when changes in the outlet temperature of the coolers is performed. For Case 1, there are two sets of intercoolers: among the mechanical compressors of air and the electric compressors of oxygen, while for Case 2, there are only one set for mechanical compressors.

For Case 1, the outlet temperature of the first cooler among the mechanical compressors of air is varied between 25 °C to 55 °C, while for the second cooler, its outlet temperature is varied between 25 °C until the extracted heat is zero, removing the cooler. On the other hand, for the electric compressors of oxygen, the study is performed considering the second and third coolers. For the second cooler, the outlet temperature is varied between 25 °C to 85 °C, while for the third cooler, the range considered is 25 °C to 117 °C, that is the maximum temperature allowed that limit the electric compressor temperature below 600 °C.

For Case 2, there is only the set of coolers among the mechanical compressors, where the outlet temperature of the first cooler is varied between 25 °C to 85 °C, while the second cooler starts at 25 °C, following the same principle as for Case 1.

An optimum point of operation is obtained for each study, considering the maximum power and thermal efficiency that can be obtained for the whole system in the study.

In this sense, a fuel consumption of 16.09 kg $s^{-1}$ is considered according to the results obtained by Wimmer and Sanz [11] for the optimized base case of the Graz cycle. Besides, there is a set of indicators used to compare the performance of the studied cases as the net thermal efficiency, net power generated, and the specific energy consumed for oxygen production.

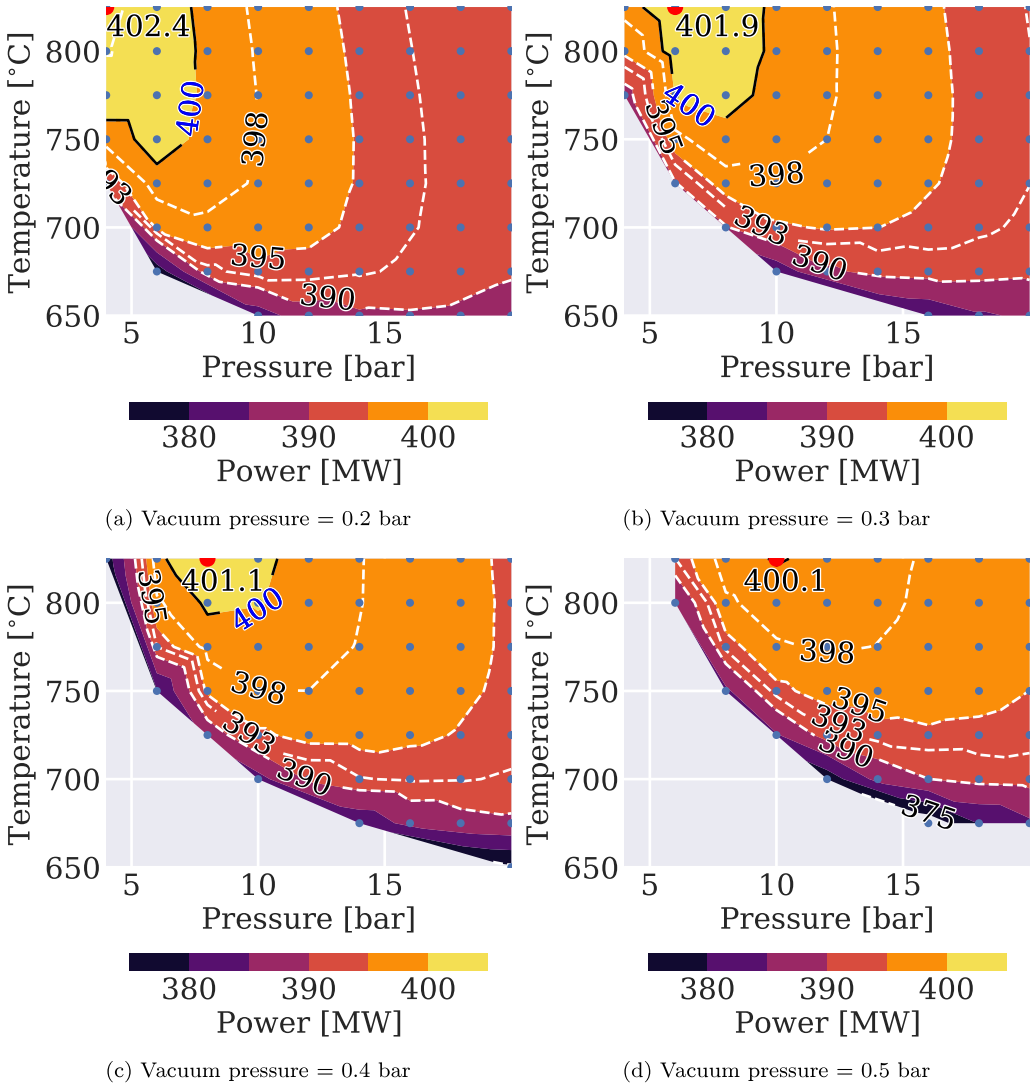


(a) Vacuum pressure = 0.2 bar

(b) Vacuum pressure = 0.3 bar

(c) Vacuum pressure = 0.4 bar

(d) Vacuum pressure = 0.5 bar

**Fig. 9.** Air feed pressure and temperature influence on net power for different vacuum pressures — Case 1.

The net thermal efficiency for the base case is determined as it is presented by Wimmer and Sanz [11]. For case 1, the net thermal efficiency is calculated as Eq. (6) states.

$$\eta_{\text{net, C1}} = \frac{\left(\sum(P_T \cdot \eta_m) - \frac{P_{C1+2}}{\eta_m}\right) \cdot \eta_{gen} \cdot \eta_{tr} - \frac{P_{C3+4}}{\eta_m} - \frac{\sum P_p}{\eta_m} - P_{aux}}{\dot{Q}_{in}} + \frac{-P_{ASU} - \frac{P_{C,O2}}{\eta_m} - P_{CPU} - \frac{P_{C\text{-}HP}}{\eta_m} - \frac{P_{C\ O2\ vacuum}}{\eta_m}}{\dot{Q}_{in}} \tag{6}$$

On the other hand, for case 2, the net thermal efficiency is calculated as Eq. (7) determines.

$$\eta_{\text{net, C2}} = \frac{\left[\sum(P_T \cdot \eta_m) - \frac{P_{C1+2}}{\eta_m}\right] \cdot \eta_{gen} \cdot \eta_{tr} - \frac{P_{C3+4}}{\eta_m} - \frac{\sum P_p}{\eta_m} - P_{aux}}{\dot{Q}_{in}} + \frac{-P_{ASU} - P_{CPU} - \frac{P_{C\text{-}HP}}{\eta_m}}{\dot{Q}_{in}} \tag{7}$$

The net power of the base case is 400 MW, where the energy consumption of the different compressors and pumps in the Graz cycle, energy losses, and consumption of auxiliary elements are considered. For the cases studied in this paper, the energy consumption of the added electric compressors is considered, as it is also seen in the net thermal efficiency equations.

Finally, for the base case, a specific energy consumption for oxygen production of 1049 kJ kg$^{-1}$, which is delivered by the cryogenic installation at 16 bar and 15 °C before reaching the CC conditions is considered, as was mentioned in Section 3.1.

For Case 1, the consumption of the electric compressor at the air line is considered, as well as the consumption of the three added compressors in the oxygen line and the heat extracted at HE-3. All these energies are used to calculate the specific energy consumption for oxygen production $E_{\text{spec,O}_2,\text{ Case 1}}$ as stated in Eq. (8).

$$E_{\text{spec,O}_2,\text{ Case 1}} = \frac{P_{C,HP} + P_{C,O2\ vacuum} + \dot{Q}_{HE\text{-}3}}{\dot{m}_{O2}} \tag{8}$$

For Case 2, the energy consumption of the electric air compressor is considered, as well as the heat extracted at HE-3, and the enthalpy flow difference of the stream used to sweep the membrane between the permeate side inlet and the HE-2 outlet, $\Delta h$. The specific energy consumption for oxygen production, $E_{\text{spec,O}_2,\text{Case 2}}$, is computed as in Eq. (9).

$$E_{\text{spec,O}_2,\text{Case 2}} = \frac{P_{C,HP} + \dot{Q}_{HE\text{-}3} + (\dot{m}h)_{PS\ \text{inlet}} - (\dot{m}h)_{HE\text{-}2\ \text{outlet}}}{\dot{m}_{O2}} \tag{9}$$

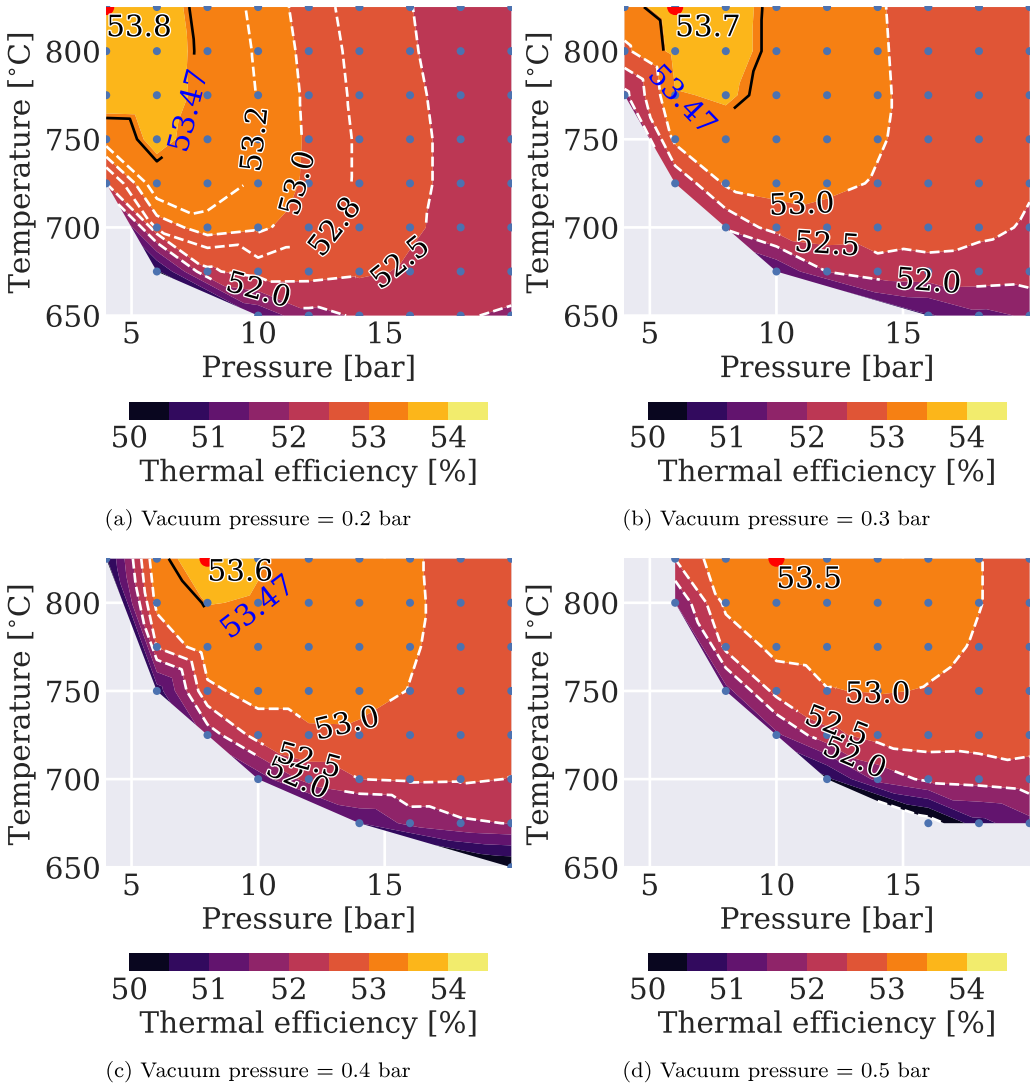


(a) Vacuum pressure = 0.2 bar

(b) Vacuum pressure = 0.3 bar

(c) Vacuum pressure = 0.4 bar

(d) Vacuum pressure = 0.5 bar

**Fig. 10.** Air feed pressure and temperature influence on cycle thermal efficiency for different vacuum pressures — Case 1.

## 4. Results

### 4.1. Case 1

#### 4.1.1. Area

Fig. 6 shows how the increase of the membrane area improves the performance of the whole cycle as the net power produced increases. The air flow to produce the required oxygen for the cycle decreases as the membrane capability for air separation is enhanced, reducing the electric air compressor power consumption and the heat exchanged in HE-3 from the HTT turbines. This trend is clearly exhibited in Fig. 7 for the mentioned variables.

However, there is an asymptotic behavior in the energy consumption and air mass flow needed for oxygen production due to a consequent reduction in the recovered thermal energy and the available enthalpy in the expansion stages, as the oxygen-depleted mass flow is also reduced.

Fig. 8 shows the specific power change related to membrane area, which decreases with larger areas. At 170 000 $m^2$, adding 1000 $m^2$ of area results in no more than 0.05 MW of added power. This size is selected for this case, being a value from which the membrane area addition does not create significant benefits to the cycle in terms of power and efficiency, and creating difficulties related to costs and facility complexities. It also allows the system to properly work in most of the proposed operation points of the proposed studied ranges for pressure and temperature for this case.

#### 4.1.2. Air feed pressure, temperature and vacuum pressure influence on performance

In Figs. 9 and 10 an optimum of net power and thermal efficiency at a pressure of 4 bar at the inlet feed side of the membrane, a temperature of 825 °C, and vacuum pressure at the oxygen line of 0.2 bar can be observed. A value of 402.4 MW net power and 53.80 % thermal efficiency are reached, 2.4 MW and 0.33 % points higher than for the baseline case, respectively.

The optimum power values for each value of vacuum pressure are found at relatively low pressures and high temperatures (825 °C). It is seen that the power is reduced as the vacuum pressure in the oxygen line increases. This trend is explained by considering the air mass flow in the oxygen production cycle, the heat in HE-3, and the electric power consumption.

An increase in the pressure and temperature at the inlet of the feed side of the membrane is beneficial for its permeability. Therefore, less air mass flow is required, as seen in Fig. 11, to extract an approximately constant oxygen amount, as the same fuel mass flow is considered.

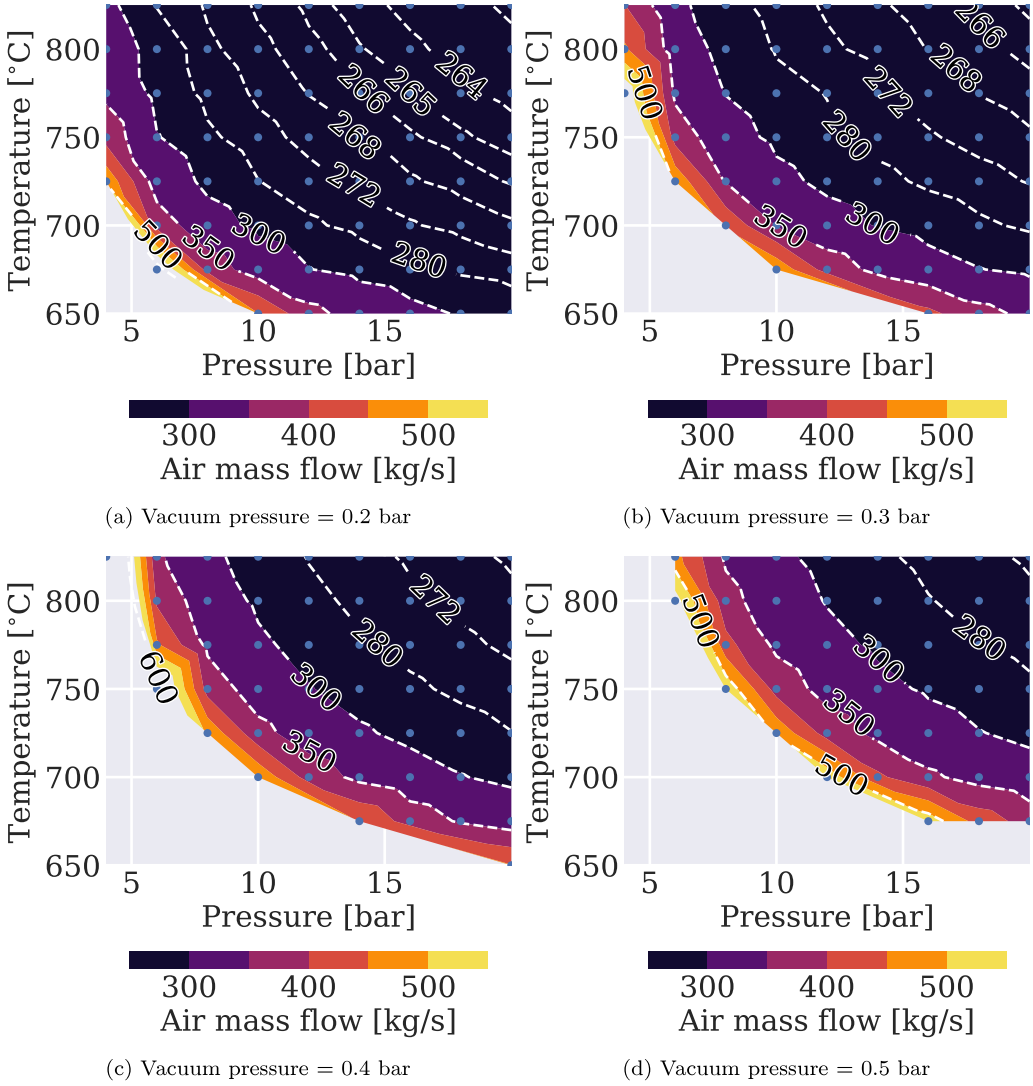


**Fig. 11.** Air feed pressure and temperature influence on air mass flow of the oxygen production cycle for different vacuum pressures — Case 1.

The latter has an effect on the consumed energy in the oxygen production cycle, for both heat exchanged in HE-3 and the electric power consumption, as it is shown in Figs. 12 and 13.

For HE-3, less heat is needed at higher pressures and lower air temperatures at the inlet feed side of the membrane. At these conditions, medium air mass flows are found, and low temperature increases are needed. However, a minimum of heat exchange in HE-3 is found for each constant value of air pressure at the membrane inlet. When low air temperatures are required, there is an increase in the air mass flow, which dominate the heat demand in this cases. On the other hand, the air mass flow is reduced at higher temperatures, and the thermal energy is now increased due to a higher variation in HE-3 of the air temperature. Then, there is a trade-off between the air mass flow to be heated and the temperature increase, which affect the energy demand in HE-3. In addition, as the pressure is reduced, a pronounced increment in the air mass flow is obtained, leading to a higher heat demand at HE-3.

There is a constant component for each vacuum pressure at the permeate side of the membrane for the electric power consumption, corresponding to the compression work at the oxygen line required to drive the oxygen mass flow from the vacuum to 16 bar. Therefore, the electric consumption variation responds to air electric compressor work changes.

A minimum of electric consumption is found for constant air temperature values at the membrane feed side. At low feed pressures, there are higher air mass flows which leads to increase the air electric compressor power. In contrast, the compression ratio acquires more importance in the compressor work for high pressures. As it was obtained for the HE-3 heat demand, there is a trade-off between the air mass flow and the compression ratio of the air electric compressor.

Thus, as the feed air temperature is reduced, the electric consumption levels are increased, where the lower membrane permeability is affected, demanding a higher air stream for oxygen production.

Given the above, the power optimum for each constant vacuum pressure is found at 825 °C, and air pressures lower than 10 bar. High temperatures dominate the membrane permeability, leading to a decrease in the required air for oxygen production. The latter allows maintaining the heat exchanged in HE-3 at reasonable values, although there is a high-temperature change.

In addition, medium-to-low pressures lead to minimum electric consumption, where the driven air is not much higher than for high pressures, and the low compression ratios reduce the energy required.

Moreover, lower vacuum pressures improve the membrane performance, for which lower pressures at the feed side of the membrane can be implemented to produce a determined oxygen amount. Although there is an increase in the oxygen line compressor work due to an

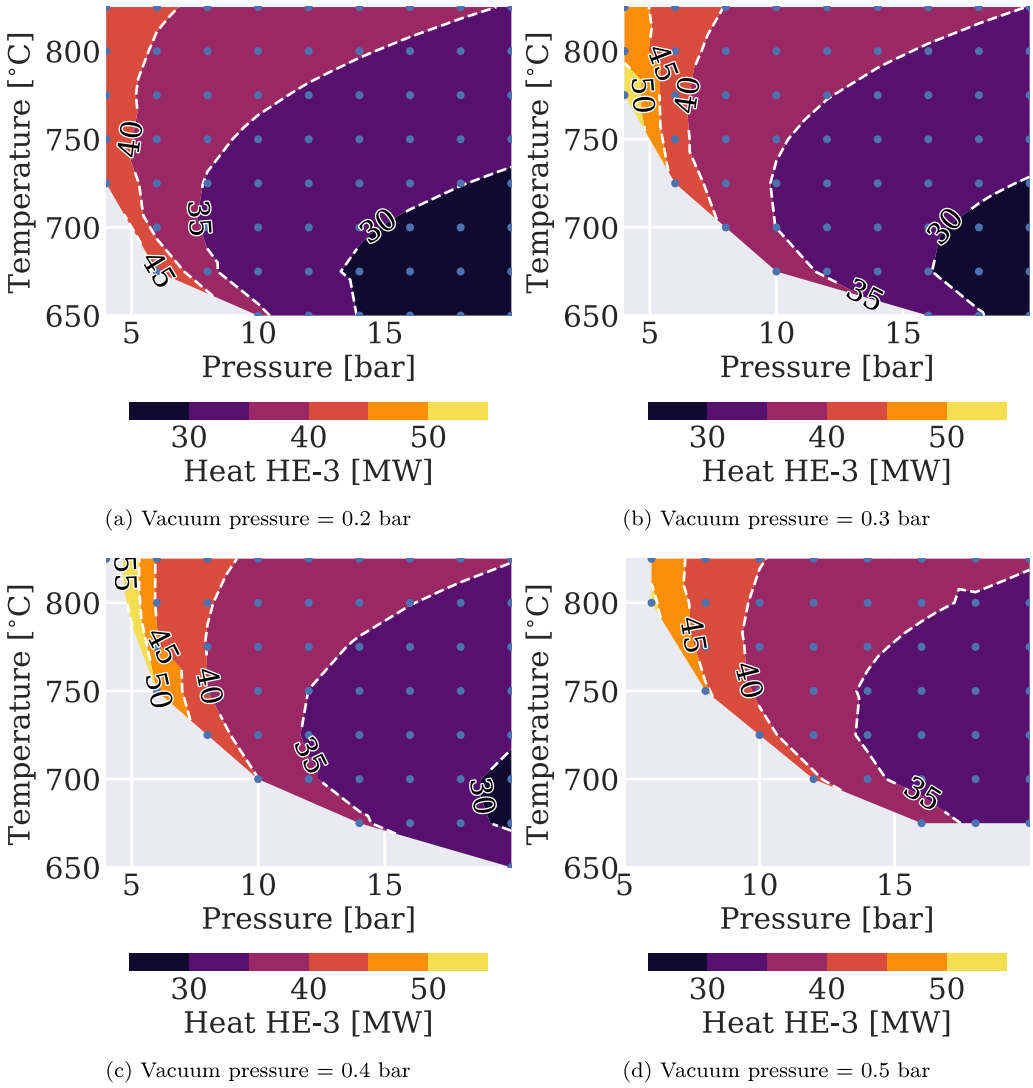


(a) Vacuum pressure = 0.2 bar

(b) Vacuum pressure = 0.3 bar

(c) Vacuum pressure = 0.4 bar

(d) Vacuum pressure = 0.5 bar

**Fig. 12.** Air feed pressure and temperature influence on heat exchanged in HE-3 for the oxygen production cycle for different vacuum pressures — Case 1.

increase in the compression ratio to reach 16 bar, the air mass flow reduction and the consequent decrease in the air electric compressor compensate for this.

It has to be highlighted that, under this reasoning, the increase of the vacuum pressure generates an increment in the gray zones of the figures, where operation is non-viable due to the low permeability of the membrane.

### 4.2. Case 2

#### 4.2.1. Area

As shown for the area variation in Case 1, an area increment enhances the system performance, as seen in Fig. 14. Mainly, the reduction of air mass flow driven through the compressors due to a membrane operation improvement reduces the power consumption of the electric air compressor and the heat exchange in HE-3, as it is seen in Fig. 15.

However, there is an asymptotic behavior as the membrane area is increased. The energy exchanged at HE-1 and HE-2 is reduced, as well as the available enthalpy at the inlet of the expansion stages. In addition, the enthalpy difference of the $O_2$/RFG increases, reducing the heat exchanged at SH1 to superheat the steam. Therefore, the net power produced for the system is affected.

A membrane area of 1 600 000 $m^2$ is selected, where further increments produce no significant benefits in terms of power and efficiency, also generating more difficulties in terms of costs and facility complexities. Fig. 16 shows that adding further 1000 $m^2$ of membrane area increases the power production only by 0.01 MW. In addition, as for Case 1, the selection of this membrane size allows the system to work suitably in most of the operation points proposed in the studied range for this case.

#### 4.2.2. Air feed pressure and temperature influence on performance

An optimum value of power and efficiency is observed for an air supply at 20 bar and 775 °C, reaching 414.17 MW and 55.35 % of thermal efficiency, 14.17 MW and 1.88 % points higher than the base case, as shown in Fig. 17.

Higher power output values are found at high pressures and medium temperatures within the studied range. The driven air mass flow through the oxygen production cycle, the consumption of electric power, heat transfer at HE-3, and the enthalpy difference of the streams at the permeate side explain this trend, as it is seen in Fig. 18.

The driven air mass flow highly depends on the feed side pressure, with higher mass flows than in Case 1 and more pronounced increments. Higher feed pressures and temperatures imply an increase in membrane permeability, causing a reduction in the air mass flow

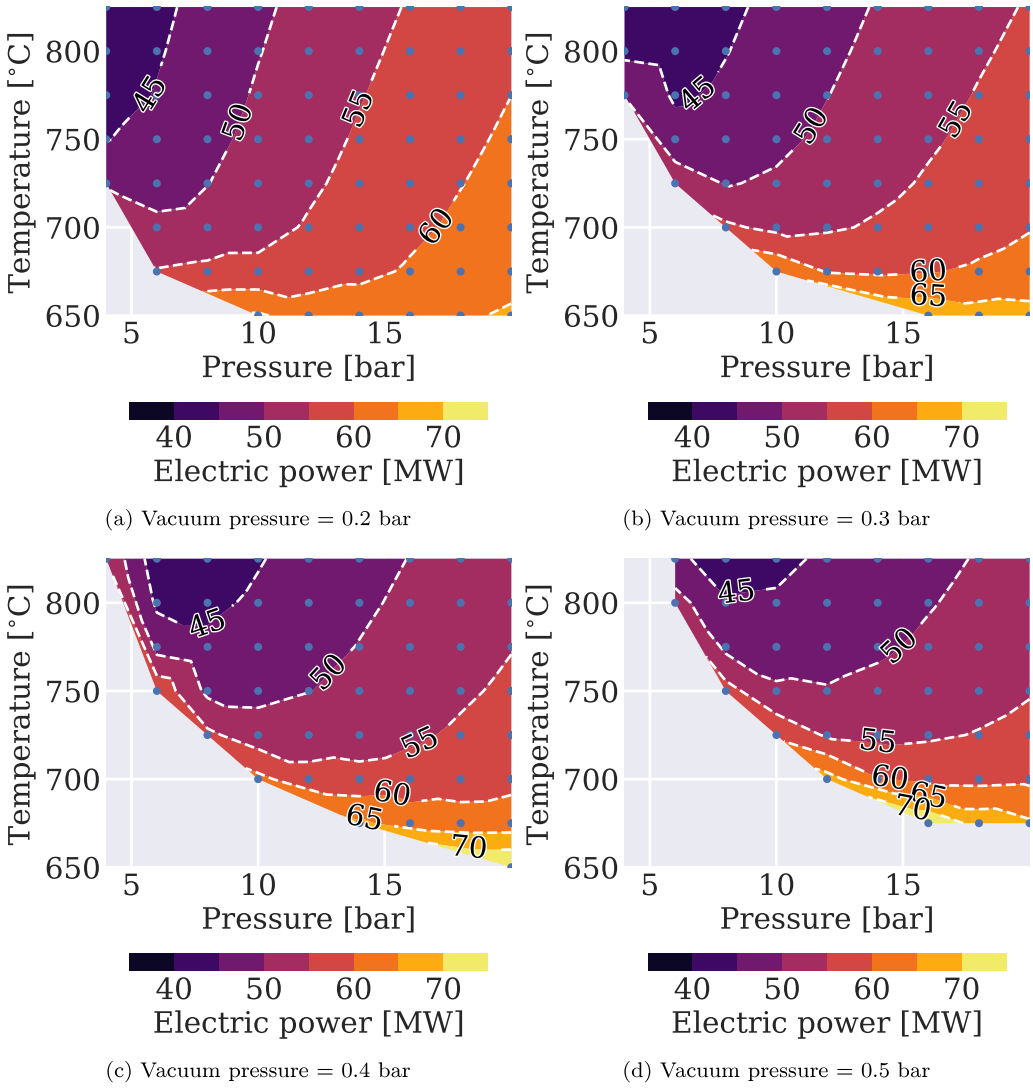


(a) Vacuum pressure = 0.2 bar

(b) Vacuum pressure = 0.3 bar

(c) Vacuum pressure = 0.4 bar

(d) Vacuum pressure = 0.5 bar

**Fig. 13.** Air feed pressure and temperature influence on electric power consumption at the oxygen production cycle — Case 1.

but also influencing both heat transfer at HE-3 and the electric power consumption.

For the heat extracted at HE-3, when the feed side pressure is kept constant, there is a significant rise in the thermal energy as the feed air temperature increases, whereas air mass flow does not vary significantly. Nevertheless, the feed side pressure variation leads to strong changes in the transferred heat due to the increased air mass flow.

Similar trends occur for the electric energy consumption, which only corresponds to the electric air compressor located upstream of the membrane feed side due to the operation mechanism of the 4-end membrane. A lower feed side pressure naturally results in a lower compression ratio of the electric compressor. However, the energy consumption is highly influenced by the change of air mass flow.

For $\Delta h$, it is necessary to define the effective temperature of oxygen production, which is the operating temperature considered for the membrane obtained from an energy balance of the membrane streams.

As an isothermal model is implemented in this study, both outlet streams from the feed and permeate sides are delivered at the same temperature. This effective temperature is shown in Fig. 19 for the whole studied range in Case 2.

Higher values of the effective temperature for oxygen production are found at low values of pressure and high temperatures at the feed side, as a higher air enthalpy flow is seen under these conditions. Consequently, there is a higher enthalpy at the HE-2 outlet of the $O_2$/RFG. Therefore, this enthalpy flow is exploited to increase the steam temperature at HPT inlet in the heat exchanger SH1 of the HRSG, increasing the power produced in the Graz Cycle.

In this sense, the power output optimum for Case 2 is found by a low electric consumption due to the high-pressure operation at the feed side inlet, which causes a reduction in the air mass flow that affects the power consumption. Additionally, this optimum power operation point achieves medium values of extracted heat at HE-3 and of the permeate side flow enthalpy difference. Medium air temperature at the feed side is obtained, not leading to an excessive heat exchange and allowing a considerably high $O_2$/RFG enthalpy flow to contribute to the HPT power production.

### 4.3. Compression intercooling optimization

#### 4.3.1. Case 1

In this part of the study, the air mass flow driven through the compressors is kept constant. An optimum of power and net efficiency is obtained by maintaining the outlet temperature of the first air cooler at 25 °C and removing the second air cooler, which leads to a temperature of 70 °C before the third compression stage.

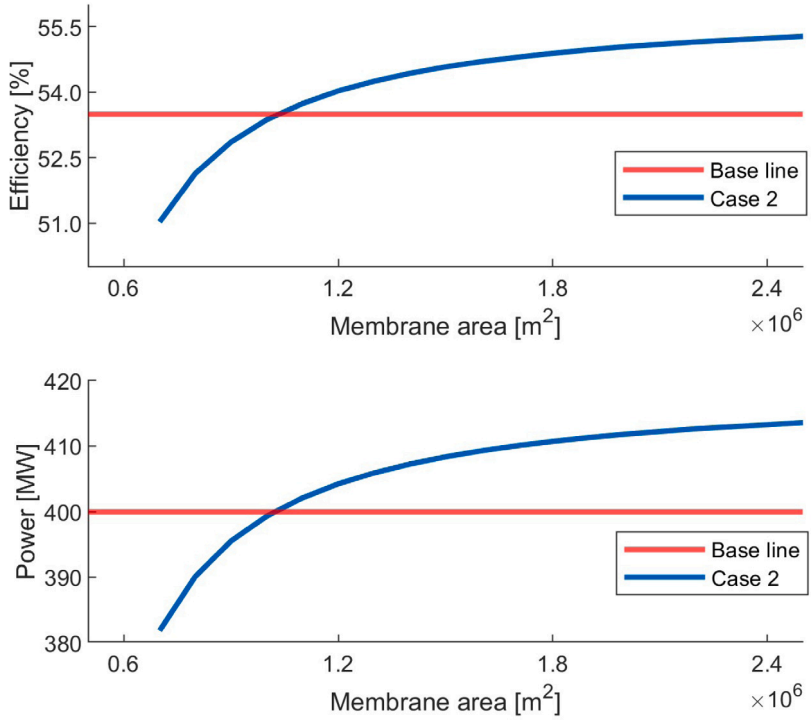


**Fig. 14.** Thermal efficiency and power variation with membrane area — Medium conditions — Case 2.

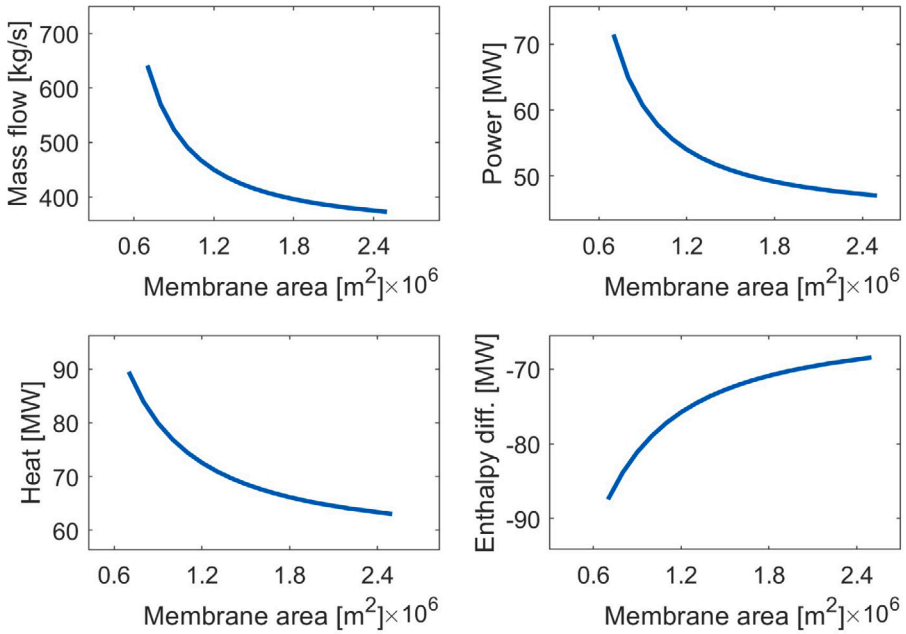


**Fig. 15.** Variation of mass flow, electric power, heat from GC and enthalpy difference on permeate side with membrane area — Medium conditions — Case 2.

A power of 403.89 MW and a net efficiency of 53.9 % is achieved, an increase of 1.5 MW and 0.2 % points of efficiency concerning Case 1 without intercooling optimization for the air compressors, as seen in Fig. 20.

When the outlet temperature of the first cooler is kept constant, an increase in the net efficiency and power production of the whole cycle is observed while the outlet temperature from the second cooler increments. Although an increase in the outlet temperature of the second cooler affects the required power in the third stage of the mechanical compression and the electric compressor, as it is seen in Fig. 21(a), there is a higher temperature after the compression stages, which has two positive effects:

- First, there is an increase in the temperature at the expansion stages, so that there is more available energy for the air compression, reducing the power increment of the electric air compressor.
- Second, a slight increase in the air temperature upstream of HE-3 diminishes the extracted heat from the HTT turbine, contributing to a rise in the produced power of this turbine.

On the other hand, when the outlet temperature of the first cooler increases, the performance of the second mechanical compressor is also

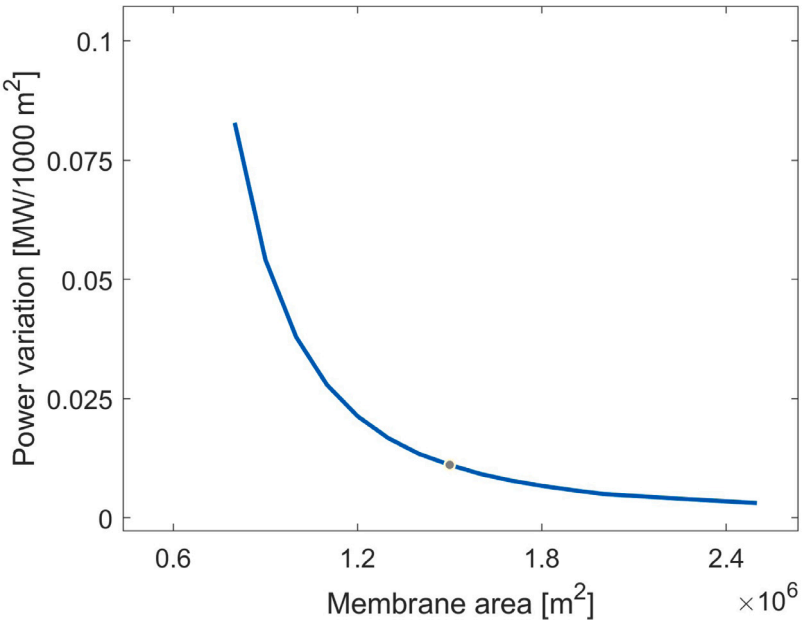


**Fig. 16.** Change of power increase with membrane area — Medium conditions — Case 2.

affected, which finally impacts the power demand of the electric air compressor. This finally affects the power and efficiency of the whole cycle.

It should be noticed that the wiggles in the isolines of electric power consumption in Fig. 21(a) are due the removal of the second cooler and thus its pressure losses, which slightly changes the trend in the power consumption.

Additionally, an optimization in Case 1 for the compressor intercooling at the oxygen line is done, where the variation of the second and third cooler outlet temperatures are considered. A power and net efficiency optimum is obtained operating with an outlet temperature of the second and third cooler of 25 °C and 117 °C, considering a limit of 600 °C for the compressors, an output power of 404.67 MW and 54.08 % of net efficiency are achieved, increasing the power by 0.77 MW and the thermal efficiency by 0.1 % points compared with the results of the first intercooling optimization process, as it is seen in Fig. 22.

An increment in the power and efficiency of the whole cycle is observed as the outlet temperature of the third cooler is increased, while the outlet temperature for the second cooler remains constant.

Although there is a power consumption increment in the electric compressor of the oxygen line due to a compression performed at a higher temperature, as seen in Fig. 23(a), the oxygen that goes into the CC also has a higher temperature, as shown in Fig. 23(b). This adds extra enthalpy to the energy balance of the combustion process which improves the cycle performance, increasing its power production. This effect will be discussed in Section 5.

On the other hand, an increase in the outlet temperature of the second cooler results in a rise in the power required at the compression stages needed to reach the pressure required at the CC, which affects the net power production.

#### 4.3.2. Case 2

For Case 2, the intercooling optimization leads to an optimum power and net efficiency of 417.24 MW and 55.76 %, an increase 3 MW and 0.41 % points with respect to Case 2 without the intercooling optimization. This optimum point is found as the outlet temperature of the first cooler is kept at 25 °C, and the second cooler is removed, reaching a temperature at the third mechanical compressor inlet of 125 °C, as seen in Fig. 24.

An increase in the required electric power with increasing the outlet temperature of the second cooler is observed in Fig. 25(a) when the outlet temperature of the first cooler is kept constant. This occurs due to performing the compression processes at a higher temperature. Nevertheless, there is an increase in the outlet temperature of the electric compressor, as in Case 1, which generates a subsequent enthalpy rise at the expansion stages inlet, leading to reductions in the increment of the electric power requirements.

Additionally, there is an increase in the available energy of the $O_2$/RFG from the HE-2 outlet, shown in Fig. 25(b), which leads to a higher contribution in the steam superheating before HPT, increasing the power production of the system.

Alternately, increasing the outlet temperature of the first cooler affects the operation of the second stage of the mechanical compression, which affects the electric energy consumed and, finally, the power production of the whole cycle.

## 5. Discussion

In Table 4, it is observed a comparison of the main variables of the oxygen production cycles of the studied cases. It is seen that for Case 1, there is considerably more specific work required for the oxygen production when compared with the base case. For Case 2, this specific work is lower when the consumed energy for the oxygen production is considered. However, the net power production for Case 1 is higher than for the base case of the Graz Cycle using cryogenic methods for oxygen production. This is achieved by the energy integration of the membrane cases.

The oxygen temperature at the inlet of the CC is higher for both membrane cases, as it is seen in Table 4, so that there is an added enthalpy flow, improving the combustion process. The effects of these improvements are seen by considering the whole energy balance of the different involved turbomachines in the systems and the differences among the mass flow driven through the different turbines and compressors, as it is seen in Tables 5 and 6 respectively.

For Case 1, there is a reduction in the steam mass flow through HPT when compared with the base case due to a decrease in the temperature of the HTT outlet flow that previously exchanged heat in HE-3. Considering the thermodynamic conditions at HPT inlet (170 bar, 599 °C), the steam mass flow is reduced. On the other hand, the recirculated working fluid flow is increased because a higher flow of a thermal buffer to the CC is required to regulate the outlet temperature of the CC, due to the mentioned increase in the enthalpy contribution of

**Table 4**
Oxygen production comparison between cases.

| | Case 1 | Case 1 optimized refrigeration | Case 2 | Case 2 optimized refrigeration | Base case |
|---|---|---|---|---|---|
| $\dot{Q}_{HE-3}$ [MW] | 43.42 | 41.21 | 61.75 | 61.93 | *** |
| $\dot{W}_{elec}$ [MW] | 40.93 | 44.01 | 47.90 | 48.60 | *** |
| $\Delta h$ [MW] | *** | *** | −69.56 | −76.20 | *** |
| $\dot{m}_{O_2}$ [kg s$^{-1}$] | 60.37 | 60.37 | 60.49 | 60.51 | 62.50 |
| $O_2$ purity [%] | 100 | 100 | 100 | 100 | 96.65 |
| $O_2$ spec. energy [kJ kg$^{-1}$] | 1397 | 1412 | 663 | 567 | 1049 |
| $O_2$ temp. at inlet CC [°C] | 414 | 599 | 599 | 599 | 150 |

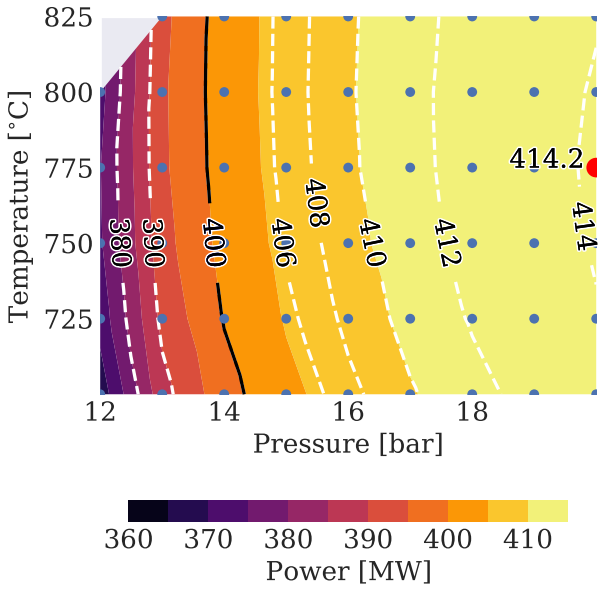


(a) Air feed pressure and temperature influence on net power cycle - Case 2

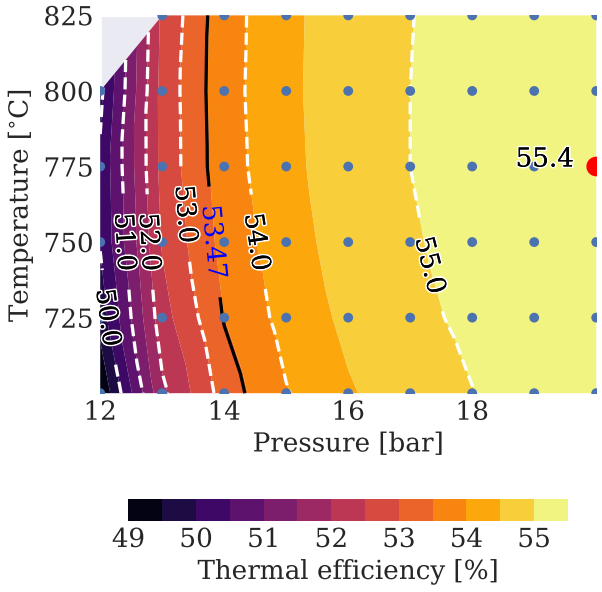


(b) Air feed pressure and temperature influence on thermal efficiency of the cycle - Case 2

**Fig. 17.** Air feed pressure and temperature influence on Graz Cycle performance — Case 2.

the oxygen flow. For these reasons, the power generated in HPT is decreased, due to the lower steam mass flow, while the compression power of C1/C2 is increased as more recirculated mass flow is needed.

For Case 2, there is an increase in HPT steam mass flow due to the additional heating from the $O_2$/RFG flow in the SH1 heat exchanger . As the thermodynamic conditions of HPT inlet are imposed, the steam mass flow is increased consequently. However, as for Case 1, the HTT outlet temperature is decreased, but this is compensated by the $O_2$/RFG heating. At the same time, the amount of recirculated working fluid needed to control the CC temperature is diminished, reducing the power consumption of C1. However, the flow of C2, which further compresses the membrane permeate outlet flow, also contains the produced oxygen, so that its power consumption rises.

Similarly, there is more power output in the first two HTT partial turbines when Case 1 and the base case are compared due to a higher mass flow through them for Case 1. For Case 2, the power output for these partial turbines is still higher than base case, where the power output of the first HTT partial turbine is higher due to the increase in C1/C2 power consumption due to the presence of oxygen in the recirculated mass flow, while for the second HTT partial turbine a higher power output is required to compensate the power output reduction in the third partial turbine.

This reduction in the power output of the third partial turbine is due to the energy loss in HE-3 for oxygen production, which is found in both membrane cases, generating a significant difference in its power output when comparing membrane and base cases. Considering that C1/C2 are driven by HTT-1, the net power output from the turbines is lower for the membrane cases.

Nevertheless, the performance improvement for the membrane cases is found in the power consumption for oxygen production. There is a high power consumption to produce oxygen at 16 bar for the base case, which is reduced considerably for the membrane cases. However, the oxygen compression to reach CC conditions requires more power for membrane cases because it is performed at a higher temperature.

At the same time, for Case 2, an additional fact diminishes the electric consumption, which is the removal of the oxygen compression stage towards the CC, whose pressure rise is performed in C2 with the recycled gas.

On the other hand, for the intercooling optimization in Case 1, there is an improvement in the net power output due to two factors: First, there is a decrease in the heat extracted in HE-3, a result of the first intercooling optimization, which allows an increase in the power output of the third HTT partial turbine. On the other hand, there is an increase in the steam mass flow as there is more available energy at HTT outlet, increasing the power output of HPT. Second, the inlet temperature of the oxygen at CC is increased due to the second intercooling optimization, which leads to increase the recirculated working fluid flow, reducing the combustion temperature, as well as the power output of the first and second HTT partial turbines.

For the intercooling optimization in Case 2, the increase in the enthalpy difference of the permeate side flow lead to more available energy in the heat exchanger SH1 of the HRSG, increasing the steam flow and, consequently, the power output of HPT. Additionally, a reduction in the recirculated working fluid flow decreases the power output at the first HTT partial turbine, which leave more available

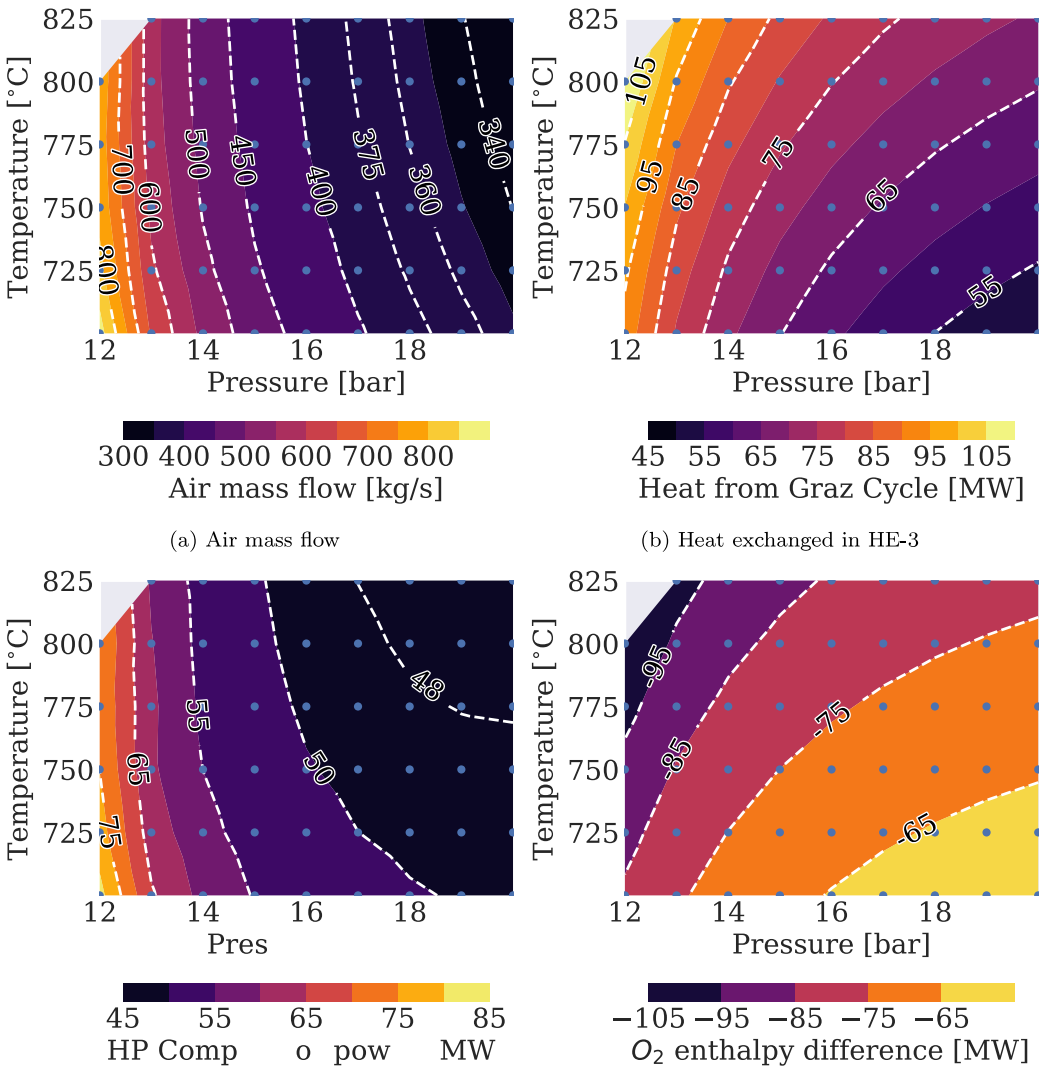


(a) Air mass flow

(b) Heat exchanged in HE-3

(c) Electric power consumption

(d) Enthalpy difference of permeate side

**Fig. 18.** Air feed pressure and temperature influence on oxygen production cycle variables — Case 2.

**Table 5**
Streams at Graz cycle.

| | Case 1 | Case 1 optimized refrigeration | Case 2 | Case 2 optimized refrigeration | Base case |
|---|---|---|---|---|---|
| Captured $CO_2$ stream [kg s$^{-1}$] | 43.80 | 43.80 | 43.92 | 43.94 | 45.94 |
| $CO_2$ purity [%] | 97.28 | 97.01 | 97.28 | 96.97 | 92.74 |
| $H_2O$ stream [kg s$^{-1}$] | 100.12 | 102.63 | 121.02 | 124.18 | 108.2 |
| $H_2O$ stream HTT cooling [kg s$^{-1}$] | 27.29 | 27.90 | 26.34 | 26.46 | 30.24 |
| $H_2O$ stream CC inlet [kg s$^{-1}$] | 72.84 | 74.74 | 94.68 | 97.71 | 77.96 |
| Recycled stream [kg s$^{-1}$] | 187.40 | 190.50 | 218.70 | 214.01 | 174.90 |
| % $H_2O$ | 75.25 | 75.60 | 56.93 | 56.06 | 75.91 |
| % $CO_2$ | 24.13 | 23.79 | 15.60 | 15.22 | 22.39 |
| % $N_2$ | 0.13 | 0.12 | 0.08 | 0.08 | 0.40 |
| % $O_2$ | 0.49 | 0.48 | 28.02 | 28.64 | 0.48 |
| CC outlet stream [kg s$^{-1}$] | 336.70 | 341.70 | 329.47 | 327.81 | 331.45 |
| Stream HTT1 outlet [kg s$^{-1}$] | 354.49 | 359.92 | 346.31 | 344.64 | 351.25 |
| Stream HTT3 outlet [kg s$^{-1}$] | 363.99 | 369.60 | 355.81 | 354.28 | 361.69 |

energy at the second stage, increasing the power output. In addition, the required power of the electric air compressor is increased due to a performance at a higher temperature.

It is important to remark that the oxygen production for all the cases is not the same as the amount of recirculated oxygen varies according to the explained differences in the studied scenarios. This recirculated flow has a small amount of oxygen because the combustion is performed with 3 % of oxygen excess to guarantee the proper fuel burning. For this reason, there is a slight deviation of oxygen production that ensures the required oxygen mass flow at the CC inlet.

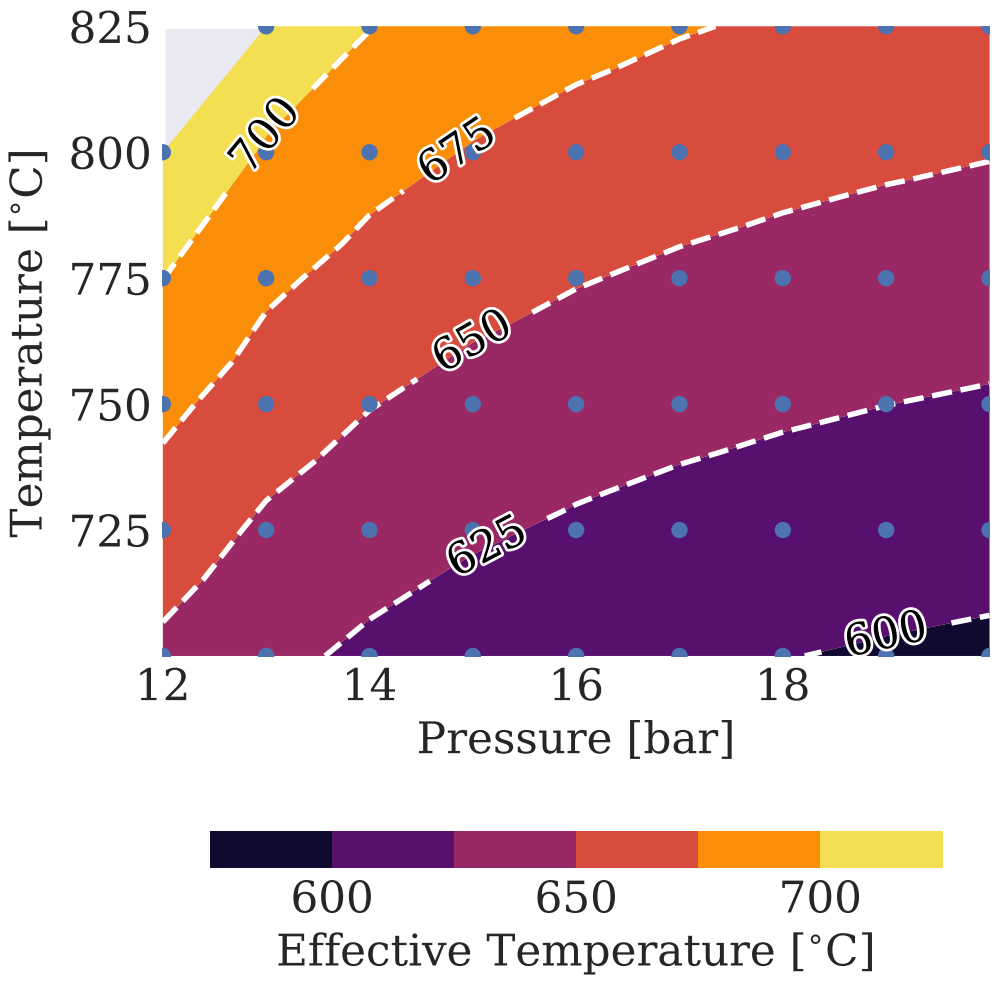


**Fig. 19.** Air feed pressure and temperature influence on effective temperature — Case 2.

**Table 6**
Power balance for the different studied cases.

| | Case 1 | Case 1 optimized refrigeration | Case 2 | Case 2 optimized refrigeration | Base case |
|---|---|---|---|---|---|
| Heat input [MW] | 748.22 | 748.22 | 748.22 | 748.22 | 748.06 |
| Turbine power [MW] | 697.07 | 709.74 | 693.36 | 692.68 | 704.70 |
| HTT-1 [MW] | 194.17 | 197.80 | 183.67 | 179.04 | 181.72 |
| HTT-2 [MW] | 249.45 | 253.20 | 256.97 | 259.93 | 251.69 |
| HTT-3 [MW] | 158.17 | 161.78 | 154.11 | 154.12 | 171.55 |
| HPT-1 [MW] | 32.54 | 33.52 | 37.63 | 38.53 | 37.67 |
| HPT-2 [MW] | 2.12 | 2.17 | 1.93 | 1.95 | 2.35 |
| LPT [MW] | 60.63 | 61.27 | 59.05 | 59.10 | 59.69 |
| Compression power [MW] | 194.17 | 197.80 | 183.67 | 179.04 | 181.72 |
| C1 [MW] | 116.72 | 118.95 | 102.85 | 100.08 | 109.56 |
| C2 [MW] | 77.45 | 78.85 | 80.82 | 78.97 | 72.16 |
| Net turbomachinery power [MW] | 493.87 | 502.76 | 500.54 | 504.41 | 513.59 |
| $CO_2$ compression [MW] | 33.14 | 33.13 | 33.09 | 33.08 | 35.11 |
| $O_2$ compression [MW] | 12.51 | 16.00 | 0.00 | 0.00 | 7.82 |
| $O_2$ prod. consumption [MW] | 40.93 | 44.01 | 47.90 | 48.60 | 65.60 |
| Water pumps [MW] | 2.28 | 2.34 | 2.76 | 2.83 | 2.47 |
| Auxiliary losses [MW] | 2.62 | 2.62 | 2.62 | 2.62 | 2.62 |
| Net power [MW] | 402.39 | 404.67 | 414.17 | 417.28 | 400.00 |
| Thermal efficiency [%] | 53.80 | 54.08 | 55.35 | 55.76 | 53.47 |

Additionally, the differences in membrane performance and size for Case 1 and 2 are studied and how this affects the trends in energy consumption for oxygen production.

In Fig. 19, it is seen that the temperature range of the membrane operation for Case 2 is between 600 and 700 °C due to the relatively low temperature of the recycled gases at the permeate side inlet of the membrane (470 °C), affecting the effective temperature of operation.

In this sense, while the optimum point of operation in Case 1 has an effective membrane temperature of 825 °C, for Case 2, this value is around 635 °C. This difference leads to two main differences in both cases:

Firstly, about the membrane size: While for Case 1, there is a membrane size of 170 000 $m^2$, an area of 1 600 000 $m^2$ was obtained for Case 2. Even though the membrane areas were also selected to operate

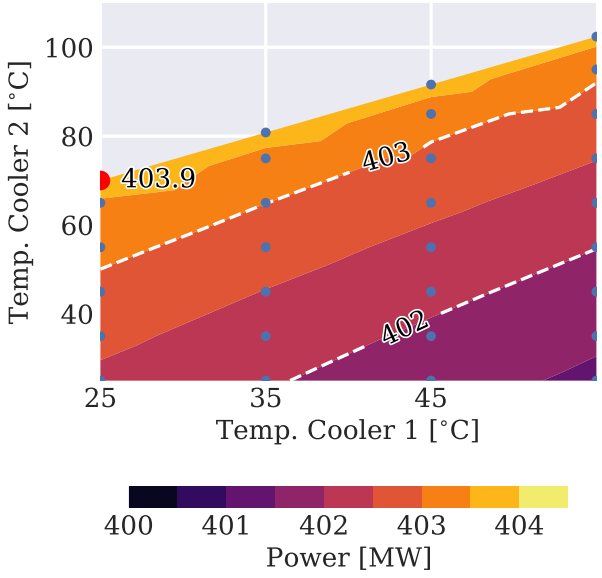


(a) Net power

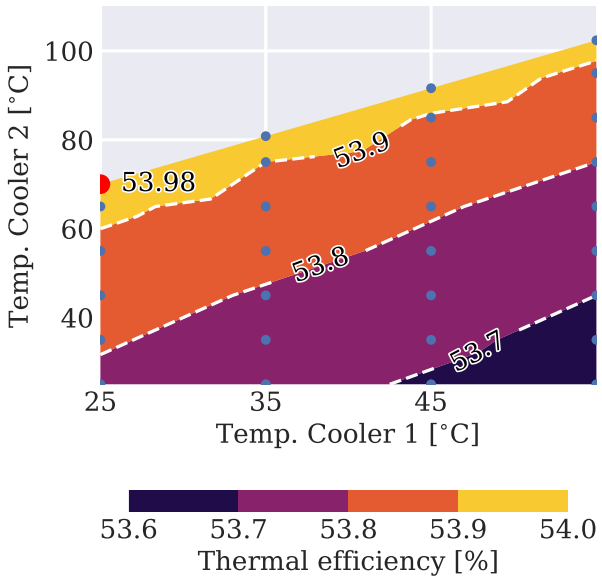


(b) Thermal efficiency

**Fig. 20.** Influence of outlet air cooler temperatures on cycle performance — Case 1.

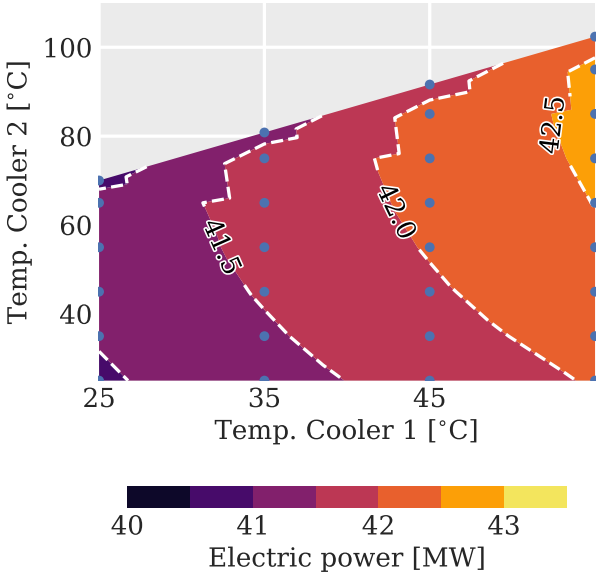


(a) Electric power consumption

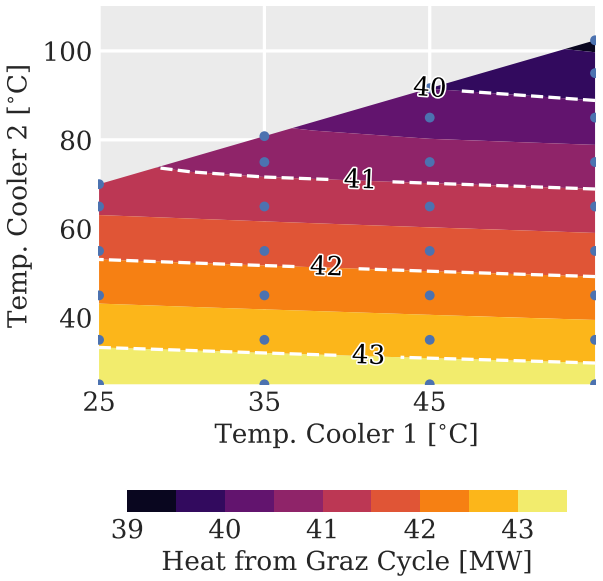


(b) Heat exchanged in HE-3

**Fig. 21.** Influence of outlet air cooler temperatures on energy consumption — Case 1.

in most of the proposed ranges of pressure and temperature of the feed air, they are also chosen in operation zones where the performance improvements are in an asymptotical region.

Secondly, about the trends concerning air mass flow, heat extracted at HE-3, and compression power: For Case 1, higher temperature levels at the membrane lead to lower air mass flow variability in the whole studied range. Nonetheless, there is a marked increase in air mass flow at low temperature and pressure zones, where membrane permeability is affected. Thus, the energy consumption is affected depending on the operation zone. As this, the heat extracted in HE-3 increases due to a higher air mass flow or temperature variation, while the air compression power increases depending on the air mass flow or the compression ratio at the air electric compressor. This is not the behavior for Case 2, where the lower levels of effective temperature at the membrane cause the air mass flows in the different zones to be higher, with a steep increase in less favorable zones for oxygen production. Hence, there is a greater dependence on air mass flow regarding the energy consumption in HE-3 and the air electric compressor.

Overall, there is an improvement for the membrane cases due to the energetic integration that allows a higher oxygen temperature at the CC inlet, a consequence of the oxygen production nature done with MIEC membranes.

For Case 2, there is a better performance as the compression stages at the oxygen line are eliminated, and high enthalpy flow from $O_2$/RFG after HE-2 that is recovered. However, there is a technological limit due to the operation at low temperatures and high membrane areas, which is being studied by Zhu and Yang [28], where membrane fabrication for operation at low temperatures (350 °C to 700 °C) is being developed. On the contrary, Case 1 generates less net power, but it works at membrane conditions that are found in the literature.

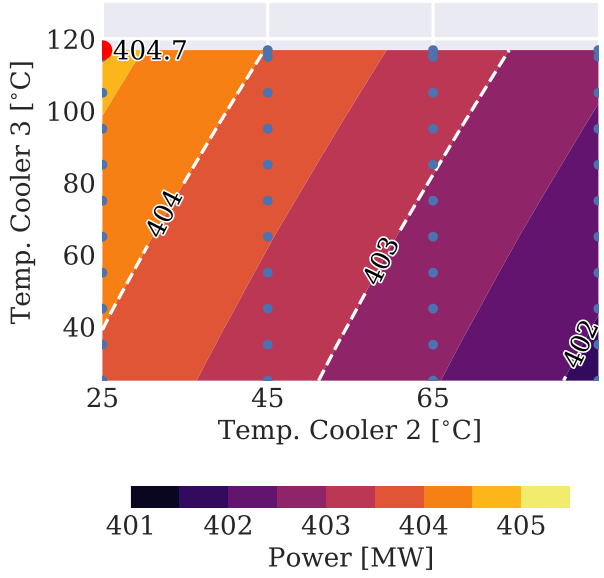


(a) Net power

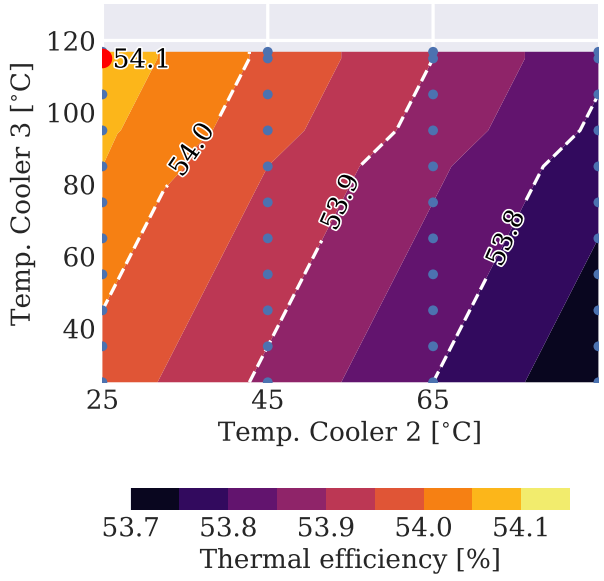


(b) Thermal efficiency

**Fig. 22.** Influence of outlet air cooler temperatures on cycle performance — Case 1.

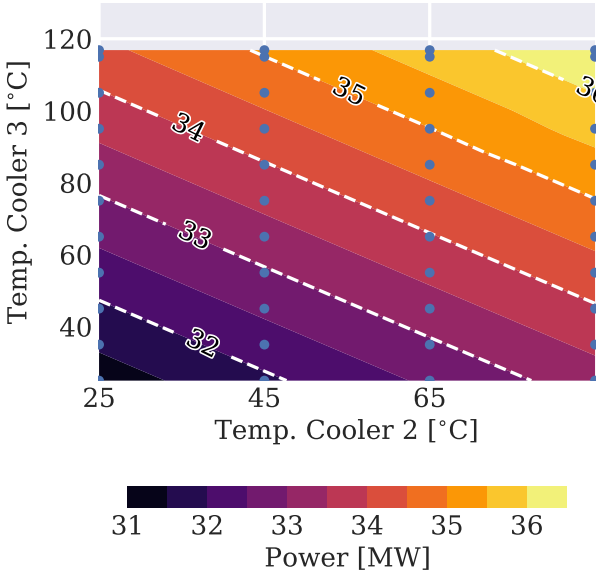


(a) Oxygen line compression power

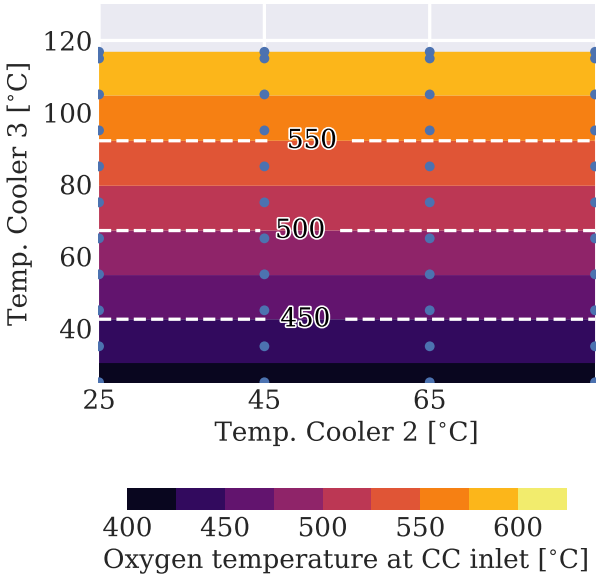


(b) Oxygen inlet temperature at combustion chamber

**Fig. 23.** Influence of outlet oxygen line cooler temperatures on oxygen production cycle variables — Case 1.

Furthermore, validation and commercial availability of these membranes for this type of application is discussed, as the oxygen production required (60.4 kg s$^{-1}$ or 5215 t d$^{-1}$) and membrane sizes (in the order of $1 \times 10^5$ m$^2$ to $1 \times 10^6$ m$^2$) require it.

First, there are studies where these membrane sizes are observed [15,29,30] which considered the same type of membranes, obtaining specific membrane areas (m$^2$ kW$^{-1}$) in the same order of magnitude as found in this study. This can be seen in Table 7. However, these are numerical studies based on reasonable membrane models.

Additionally, this technology is currently under development availability, a highly-researched topic in the industry. One of the leading organizations addressing this issue is Air Products, which is currently working on a multi-phase project. The project final phase will focus on the operation of a 2000 t d$^{-1}$ [28]. Nonetheless, the improvement of mechanical properties and larger membrane area per unit volume are required conditions for practical applications [31].

**Table 7**
Specific membrane area comparison.

| | Specific membrane area (m$^2$ kW$^{-1}$) | $O_2$ production (kg s$^{-1}$) |
|---|---|---|
| Portillo et al. [15] | 0.69 | 202.0 |
| Chen et al. [30] | 1.38 | 15.2 |
| Castillo [29] | 0.80 | 96.6 |
| Case 1 | 0.42 | 60.4 |
| Case 2 | 3.83 | 60.5 |

On the other hand, the risk due to high oxygen reactivity is a technical challenge that comes from using a high-purity oxygen stream

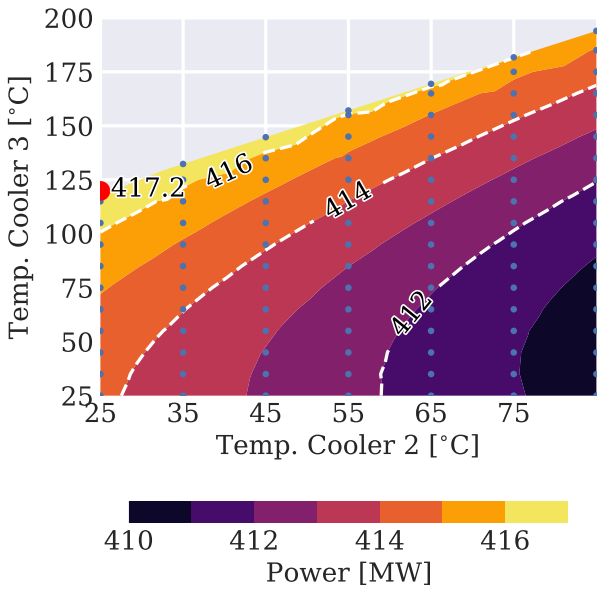


(a) Net power cycle

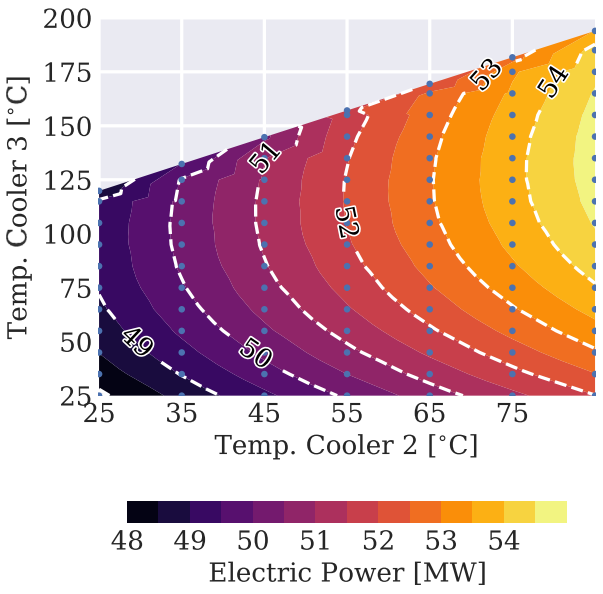


(a) Electric power consumption

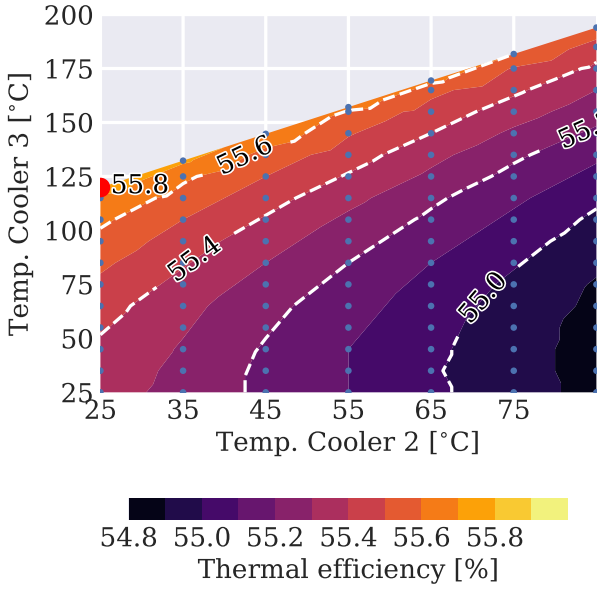


(b) Thermal efficiency

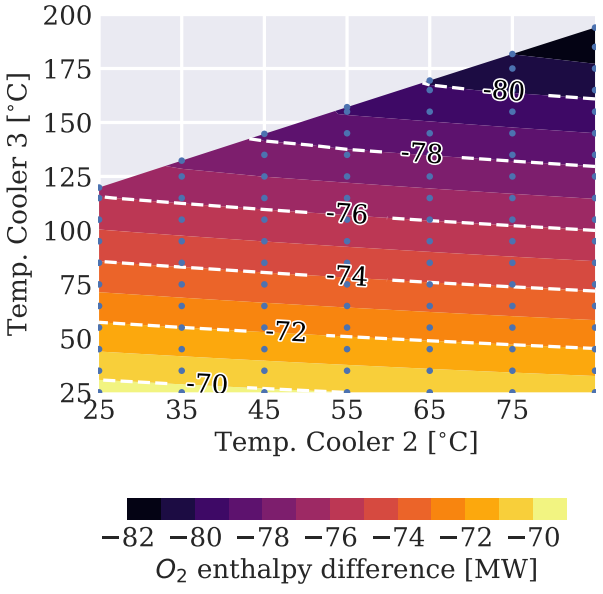


(b) Enthalpy difference of permeate side flow

**Fig. 24.** Influence of outlet air cooler temperatures on cycle performance — Case 2.

**Fig. 25.** Influence of outlet air cooler temperatures on cycle performance.

for Case 1. In Case 2, the last compression stage of oxygen is C2, performed with an O2/RFG mixture, reducing risks associated with the high reactivity of the stream. Meanwhile, for Case 1, C-O2 works with high-purity oxygen, for which special compressors are needed, as they have to be oil-free and completely sealed, according to [32]. On the other hand, as the ignition temperature of steel is about 1150 °C, temperatures below 1000 °C are acceptable under these working conditions to avoid metal firing.

## 6. Conclusions

In this paper, a thermodynamic comparison of the Graz cycle operating with two oxygen production alternatives is performed. A base case using cryogenic means and two cases where MIEC membranes are implemented, using 3-end and 4-end membranes, are contrasted.

First, the main parameters of both membrane-based cases are optimized, as well as the intercooling among mechanical and electric compressors.

For Case 1, an optimum operation was found where the net power output and thermal efficiency values are 404.67 MW and 54.08 %, respectively (4.67 MW and 0.61 % points higher than the base case), while for Case 2, a net power output and thermal efficiency of 417.24 MW and 55.76 %, respectively, were obtained (increasing 17.24 MW and 2.30 % points respect to the base case)

On the other hand, when membrane cases are compared with the base case, the oxygen production required can also be obtained using MIEC membrane cycles, leading to a energy integration that helps to improve the overall performance of the cycle

A reduction of the power output of HTT-3 due to the heat extraction in HE-3 is the main reason why the total power output of the turbines

is lower for the membrane cases compared with the turbines in the base case. Nonetheless, there is a high energy consumption for oxygen production in the base case, which markedly decreases the net power output and leads to the higher efficiency of membrane cases when the comparison is made.

Similarly, for Case 2, there is an additional increase as the oxygen line compressors are removed and a higher HPT power output than in Case 1 is obtained due to the recirculation of a high enthalpy flow from the HE-2 outlet which superheats the water steam in SH1.

Comparing both membrane cases from a technological perspective, Case 1 seems as more feasible to construct due to the favorable conditions of feed temperature and membrane size when compared with Case 2. Research is under way to create reliable membranes that operate at medium and low temperatures, which is the main technological barrier to overcome for Case 2. Additionally, special attention must be given to the high-purity oxygen compressors in Case 1, as they reach considerable temperatures with high-purity oxygen, which can be threatening due the high reactivity of the stream.

Being this said, membrane-based oxygen production cycles are shown as a promising alternative to be energetically integrated with oxy-combustion power plants, as far as technological issues are correctly addressed as membrane limitations and high-purity oxygen streams through pipelines and turbomachines.

Finally, further research is envisaged to determine the influence of the efficiency of the turbomachines on the whole cycle performance; also, an economic analysis of the studied systems is highly recommended.

## List of symbols

| | |
|---|---|
| $A$ | Membrane area |
| $C$ | Wagner conductivity constant |
| C1/C2 | Recirculating working fluid compressors |
| C3/C4 | Carbon capture compressors |
| CC | Combustion chamber |
| CCS | Carbon Dioxide Capturing and Storage |
| $\Delta h$ | Enthalpy flow difference of the stream used to sweep the membrane between the permeate side inlet and the HE-2 outlet |
| $E_{\text{spec},O_2}$ | Specific energy consumed for oxygen production |
| $\eta_{\text{gen}}$ | Electric generator efficiency |
| $\eta_{\text{m}}$ | Mechanical efficiency |
| $\eta_{\text{tr}}$ | Transformer efficiency |
| HE-1 | First heat exchanger of oxygen production cycle |
| HE-2 | Second heat exchanger of oxygen production cycle |
| HE-3 | Third heat exchanger of oxygen production cycle |
| HPT | High-pressure turbine |
| HRSG | Heat recovery steam generator |
| HTT | High-temperature turbine |
| $K$ | Wagner temperature constant |
| $L$ | Membrane thickness |
| LPT | Low-pressure turbine |
| MW | Molecular weight |
| $P_{\text{aux}}$ | Auxiliar losses |
| $P_{\text{C1+2}}$ | Recirculating working fluid compressors power |
| $P_{\text{C3+4}}$ | Carbon capture compressors power |
| $P_{\text{C,HP}}$ | High-pressure electric compressor power |
| $P_{\text{C},O_2}$ | Oxygen compressor power |
| $P_{\text{C},O_2\ \text{vacuum}}$ | Oxygen line compressors power |
| $P_{\text{CPU}}$ | Carbon capture power |
| $P_{O_2,f}$ | Oxygen feed partial pressure |
| $P_{O_2,p}$ | Oxygen permeate partial pressure |
| $P_{\text{p}}$ | Water pumps power |
| $P_{\text{T}}$ | Turbine power |
| $\dot{Q}_{\text{HE-3}}$ | Third heat exchanger power |
| RFG | Recycled flue gases |

## CRediT authorship contribution statement

**Fabio Alberto Gutiérrez:** Conceptualization, Methodology, Software, Formal Analysis, Investigation, Data curation, Writing – original draft, Writing – review & editing, Visualization, Funding acquisition. **Luis Miguel García-Cuevas:** Methodology, Software, Validation, Formal Analysis, Writing – review & editing, Visualization, Supervision, Project administration. **Wolfgang Sanz:** Methodology, Software, Validation, Formal Analysis, Resources, Writing – review & editing, Supervision, Project administration.

## Declaration of competing interest

The authors declare that they have no known competing financial interests or personal relationships that could have appeared to influence the work reported in this paper.

## Data availability

Data will be made available on request.

## Acknowledgments

Authors want to acknowledge to the institution "Conselleria de Innovación, Universidades, Ciencia *y* Sociedad Digital de la Generalitat Valenciana", Spain and its grant programs "Subvenciones para la contratación de personal investigador de carácter predoctoral" for doctoral studies (ACIF/2020/246) and "Subvenciones para estancias de contratados predoctorales en centros de investigación fuera de la Comunitat Valenciana" for doctoral stays (BEFPI/2021/038), both funded by The European Union.

## References

[1] IEA. World energy outlook 2020 report extract overview. 2021, URL: https://www.iea.org/reports/world-energy-outlook-2020?mode=overview, visited on 2021-08-04.
[2] EU. What is the source of the electricity we consume? 2019, URL: https://ec.europa.eu/eurostat/cache/infographs/energy/bloc-3b.html, visited on 2021-08-04.
[3] EU. 2050 Long-term strategy. 2018, URL: https://ec.europa.eu/clima/policies/strategies/2050_en, visited on 2021-08-04.
[4] Wilberforce T, Olabi A, Sayed E, Elasaid K, Abdelkareem M. Progress in carbon capture technologies. Sci Total Environ 2021;761:143203. http://dx.doi.org/10.1016/2020.1432034.
[5] Markewitz P, Zhao L, Ryssel M, Moumim G, Wang Y, Sattler CS, Robinius M, Stolten D. Carbon capture for CO2 emission reduction in the cement industry in Germany. Energies 2019;761:2432. http://dx.doi.org/10.3390/en12122432.
[6] IEA. Report extract: Electricity. 2021, URL: https://www.iea.org/reports/global-energy-review-2020/electricity, visited on 2021-08-04.
[7] Gunasekaran S, Mancini N, Mitsos A. Optimal design and operation of membrane-based oxy-combustion power plants. Energy 2014;46:338–54. http://dx.doi.org/10.1016/j.energy.2014.04.008.
[8] Ozsari I, Ust HK, Yasin Us Kayadelen. Comparative energy and emission analysis of oxy–combustion and conventional air combustion. Arab J Sci Eng 2021;46:2477–92. http://dx.doi.org/10.1007/s13369-020-05130-0.
[9] Shi Y, Liu Q, Shao Y, Zhong W. Energy and exergy analysis of oxy-fuel combustion based on circulating fluidized bed power plant firing coal, lignite and biomass. Fuel 2020;269:117442. http://dx.doi.org/10.1016/j.fuel.2020.117424.
[10] Liang Y, Cai L, Guan Y, Liu W, Xiang Y, Li J, Hei TH. Numerical study on an original oxy-fuel combustion power plant with efficient utilization of flue gas waste heat. Fuel 2019;193:116854. http://dx.doi.org/10.1016/j.energy.2019.116854.
[11] Wimmer K, Sanz W. Optimization and comparison of the two promising oxy-combustion cycles NET power cycle and graz cycle. Int J Greenhouse Gas Control 2020;99:103055. http://dx.doi.org/10.1016/j.ijggc.2020.103055.
[12] Cai L, Tan L, Liang Y, Yin X, Liu C, Guan Y. Numerical study on sulfur-bearing natural gas oxy-fuel combustion power plant. Appl Therm Eng 2021;196:117292. http://dx.doi.org/10.1016/j.applthermaleng.2021.117292.
[13] Wu F, Argyle MD, Dellenback PA, Fan M. Progress in O2 separation for oxy-fuel combustion–a promising way for cost-effective CO2 capture: A review. Prog Energy Combust Sci 2018;67:188–205. http://dx.doi.org/10.1016/j.pecs.2018.01.004.

[14] Arratibel Plazaola A, Cruellas Labella A, Liu Y, Badiola Porras N, Pacheco Tanaka DA, Sint Annaland MV, Gallucci F. Mixed ionic-electronic conducting membranes (MIEC) for their application in membrane reactors: A review. Processes 2019;7(3). http://dx.doi.org/10.3390/pr7030128.

[15] Portillo E, Gallego Fernandez LM, Vega F, Alonso-Farinas B, Navarrete B. Oxygen transport membrane unit applied to oxy-combustion coal power plants: A thermodynamic assessment. J Environ Chem Eng 2021;9(3). http://dx.doi.org/10.1016/j.jece.2021.105266.

[16] Skorek-Osikowska A, Bartela L, Kotowicz J. A comparative thermodynamic, economic and risk analysis concerning implementation of oxy-combustion power plants integrated with cryogenic and hybrid air separation units. Energy Convers Manage 2015;92(3). http://dx.doi.org/10.1016/j.enconman.2014.12.079.

[17] Serrano J, Martín J, Gómez-Soriano J, Raggi R. Theoretical and experimental evaluation of the spark-ignition premixed oxy-fuel combustion concept for future CO2 captive powerplants. Energy Convers Manage 2021;244:114498. http://dx.doi.org/10.1016/j.enconman.2021.114498.

[18] Sanz W, Jericha H, Moser M, Heitmeir F. Thermodynamic and economic investigation of an improved graz cycle power plant for CO2 capture. J Eng Gas Turb Power 2005;127:765–72. http://dx.doi.org/10.1115/1.1850944.

[19] Sanz W, Jericha H, Luckel F, Göttlich E, Heitmeir F. A further step towards a graz cycle power plant for CO2 capture. In: ASME turbo expo 2005: power for land, sea and air. Reno, Nevada, USA: ASME; 2005, p. 181–90. http://dx.doi.org/10.1115/GT2005-68456.

[20] Sanz W, Jericha H, Göttlich E. Design concept for large output graz cycle gas turbines. In: ASME turbo expo 2006: power for land, sea and air. Barcelona, Spain: ASME; 2006, p. 1–14. http://dx.doi.org/10.1115/GT2006-90032.

[21] Sanz W, Jericha H, Göttlich E, Neumayer F. Design details of a 600 MW graz cycle thermal power plant for CO2 capture. In: Proceedings of ASME turbo expo 2008: power for land, sea and air. Berlin, Germany: ASME; 2008, p. 507–16. http://dx.doi.org/10.1115/GT2008-50515.

[22] Sanz W, Mayr M, Jericha H. Thermodynamic and economic evaluation of an IGCC plant based on the graz cycle for CO2 capture. In: Proceedings of ASME turbo expo 2010: power for land, sea and air. Glasgow, UK: ASME; 2010, p. 493–503. http://dx.doi.org/10.1115/GT2010-22189.

[23] Sanz W, Hustad C-W, Jericha H. First generation graz cycle power plant for near-term deployment. In: Proceedings of ASME turbo expo 2011. Vancouver, British Columbia, Canada: ASME; 2011, p. 969–79. http://dx.doi.org/10.1115/GT2011-45135.

[24] Sanz W, Braun M, Jericha H, Platzer M. Adapting the zero-emission graz cycle for hydrogen combustion and investigation of its part load behaviour. In: Proceedings of ASME turbo expo 2016: turbomachinery technical conference and exposition. Seoul, South Korea: ASME; 2016, http://dx.doi.org/10.1115/GT2016-57988.

[25] SimTech. What is IPSEpro?. 2021, URL: https://www.simtechnology.com/CMS/index.php/ipsepro, visited on 2021-08-04.

[26] Catalán-Martínez D, Santafé-Moros A, Gozálvez-Zafrilla J, García-Fayos J, Serra J. Characterization of oxygen transport phenomena on BSCF membranes assisted by fluid dynamic simulations including surface exchange. Chem Eng J 2020;387:124069. http://dx.doi.org/10.1016/j.cej.2020.124069.

[27] Baumann S, Serra J, Lobera M, Escolástico S, Schulze-K"uppers, Meulenberg W. Ultrahigh oxygen permeation flux through supported $Ba_{0.5}Sr_{0.5}Co_{0.8}Fe_{0.2}O_{3-\delta}$ membranes. J Membr Sci 2011;377:198–205. http://dx.doi.org/10.1016/j.memsci.2011.04.050.

[28] Zhu X, Yang W. Mixed conducting ceramic membranes, fundamentals, materials and applications. Springer; 2017.

[29] Castillo R. Thermodynamic analysis of a hard coal oxyfuel power plant with high temperature three-end membrane for air separation. Appl Energy 2011;88:1480–93. http://dx.doi.org/10.1016/j.apenergy.2010.10.044.

[30] Chen W, Van der Ham L, Nijmeijer A, Winnubst L. Membrane-integrated oxy-fuel combustion of coal: Process design and simulation. J Membr Sci 2015;492:461–70. http://dx.doi.org/10.1016/j.memsci.2015.05.062.

[31] Bai W, Feng J, Luo C, Zhang P, Wang H, Yang Y, Zhao Y, Fan H. A comprehensive review on oxygen transport membranes: Development history, current status, and future directions. Int J Hydrogen Energy 2021;46:36257–90. http://dx.doi.org/10.1016/j.ijhydene.2021.08.177.

[32] Compressors B. What is a oxygen compressor? 2022, URL: https://www.oxygen-compressors.com/oxygen-compressor.html, visited on 2022-09-22.